Dynamics of greenhouse gases (CO_2, CH_4, N_2O) along the Zambezi River and major tributaries, and their importance in the riverine carbon budget

Cristian R. Teodoru[1], Frank C. Nyoni[2], Alberto V. Borges[3], François Darchambeau[3], Imasiku Nyambe[2] and Steven Bouillon[1]

[1] KU Leuven, Department of Earth and Environmental Sciences, Leuven, Belgium

[2] University of Zambia, Integrated Water Research Management Centre, Lusaka, Zambia

[3] University of Liège, Chemical Oceanography Unit, Liège, Belgium

Corresponding author: Cristian R. Teodoru (teo.teodoru@ees.kuleuven.be)

Abstract. Spanning over 3000 km in length and with a catchment of approximately 1.4 million km^2, the Zambezi River is the fourth largest river in Africa and the largest flowing into the Indian Ocean from the African continent. We present data on greenhouse gas (GHG, carbon dioxide (CO_2), methane (CH_4), and nitrous oxide (N_2O)) concentrations and fluxes, as well as data that allow characterizing sources and dynamics of carbon pools collected along the Zambezi River, reservoirs and several of its tributaries during 2012 and 2013 and over two climatic seasons (dry and wet) to constrain the interannual variability, seasonality and spatial heterogeneity along the aquatic continuum. All GHG concentrations showed high spatial variability (coefficient of variation: 1.01 for CO_2, 2.65 for CH_4 and 0.21 for N_2O). Overall, there was no unidirectional pattern along the river stretch (i.e. decrease or increase towards the ocean), as the spatial heterogeneity of GHGs appeared to be determined mainly by the connectivity with floodplains and wetlands, and the presence of man-made structures (reservoirs) and natural barriers (waterfalls, rapids). Highest CO_2 and CH_4 concentrations in the main channel were found downstream of extensive floodplains/wetlands. Undersaturated CO_2 conditions, in contrast, were characteristic for the surface waters of the two large reservoirs along the Zambezi mainstem. N_2O concentrations showed the opposite pattern, being lowest downstream of floodplains and highest in reservoirs. Among tributaries, highest concentrations of both CO_2 and CH_4 were measured in the Shire River whereas low values were characteristic for more turbid systems such as the Luangwa and Mazoe rivers. The interannual variability in the Zambezi River was relatively large for both CO_2 and CH_4, and significantly higher concentrations (up to two-fold) were measured during wet seasons compared to the dry season. Interannual variability of N_2O was less pronounced but higher values were generally found during the dry season. Overall, both concentrations and fluxes of CO_2 and CH_4 were well below the median/average values for tropical rivers, streams and reservoirs reported previously in literature and used for global extrapolations. A first-order

mass balance suggests that carbon (C) transport to the ocean represents the major component (59%) of the budget (largely in the form of dissolved inorganic carbon, DIC), while 38% of the total C yield is annually emitted into the atmosphere, mostly as CO_2 (98%), and 3% is removed by sedimentation in reservoirs.

1 Introduction

Contrary to the earlier perception of inland waters as simple pipelines passively transporting significant amounts of both organic and inorganic carbon (C) to the ocean, it is increasingly recognized that freshwater ecosystems are capable of processing large quantities of C derived from the surrounding landscape, being therefore active components of global C cycling. Global figures based on recent data compilations suggest that the amount of C processed and emitted into the atmosphere from inland waters offsets the overall C transport to the global ocean (Cole at al., 2007; Tranvik et al., 2009; Aufdenkampe et al., 2011; Bastviken et al., 2011; Butman and Raymond, 2011; Raymond et al., 2013). This amount of terrestrial C processed in rivers, lakes, and reservoirs reaches approximately half the magnitude of the oceanic CO_2 sink (IPCC, 2013), a value that is similar or even higher in magnitude than C uptake by terrestrial ecosystem (Aufdenkampe et al., 2011; IPCC, 2013). Despite large uncertainties related to these global estimates, it has become evident that freshwater ecosystems play a vital role in C budgets, disproportional to their areal extent (Cole at al., 2007). Quantifying the role of freshwater ecosystems as C sources and sinks, understanding the link between terrestrial and aquatic ecosystem as well as the underlying biogeochemical processes are therefore fundamental for quantitative estimates of the impact of land use-related changes in C dynamics and for improving estimates of ecosystem C budgets.

Although rivers represent key elements of freshwater ecosystems, their role in global or regional C budgets remains yet unclear. Resulting from groundwater inputs of dissolved inorganic C (DIC) and from the mineralization of terrestrial organic C (OC) (Battin et al., 2008), supersaturation in CO_2 has been reported for large rivers in boreal, temperate and tropical areas (Cole and Caraco, 2001; Richey et al., 2002; Aufdenkampe et al., 2011; Raymond et al. 2013; Bouillon et al., 2014; Abril et al., 2014; 2015). Studies of CO_2

dynamics in low-order rivers in temperate and boreal regions have also shown that these systems are extremely dynamic in terms of DIC (Guasch et al., 1998; Worrall et al., 2005; Waldron et al., 2007), and generally highly supersaturated in CO_2 (Kling et al., 1991; Hope et al., 2001; Finlay, 2003; Teodoru et al., 2009). Controlled by several biogeochemical processes (i.e. organic matter oxidation, photosynthesis and respiration, and exchange with atmosphere) and characterized by distinct isotopic signature, DIC stable isotopes (δ^{13}C-DIC) is a powerful tool which can be used to distinguish between different riverine DIC sources (i.e. atmospheric/soil CO_2 or carbonate dissolution), to trace the DIC transport to the ocean and to assess the carbon transformation in the river itself. Data on tropical rivers and streams are particularly scarce compared to other regions despite their high contribution (more than half) to the global freshwater discharge to the ocean, and particular high importance in terms of riverine transport of sediments and C (Ludwig et al., 1996; Schlünz and Schneider, 2000) and the suggested higher areal CO_2 outgassing rates than temperate or boreal rivers (Aufdenkampe et al., 2011). While our understanding of C dynamics in tropical regions comes mostly from studies of the Amazon River Basin, up to date only a handful of studies explored the biogeochemical functioning of equally important African rivers such as the Bia, Tanoé and Tanoé rivers in Ivory Coast (Koné et al., 2009, 2010), the Tana (Kenya) and the Oubangui rivers (Congo River basin) (Bouillon et al., 2009, 2012, 2014; Tamooh et al., 2012, 2013), the Congo River (Wang et al., 2013; Mann et al., 2014), and the Athi-Galana-Sabaki River (Kenya) (Marwick et al., 2014). Constraining the overall importance of rivers in the global C budget therefore requires an improved understanding of C cycling in other tropical and subtropical regions.

As part of a broader study on catchment-scale biogeochemistry of African Rivers, the present study examines the spatio-temporal dynamics of CO_2, CH_4 and N_2O concentrations and fluxes in the Zambezi River Basin based on three sampling campaigns extended over two

climatic seasons (wet 2012, wet 2013 and dry 2013). The study quantifies the magnitude of CO_2 and CH_4 concentrations and fluxes, identifies the main C sources and the controlling factors responsible for the observed patterns, and examines hotspots for GHG exchange with the atmosphere. Finally, we make a first attempt at a C mass balance for the Zambezi River over the study period budgeting emissions, sinks and transport of C.

2 Materials and Methods

2.1 The Zambezi River – general characteristics

The Zambezi River is the fourth largest river in Africa in terms of discharge after the Congo, Nile and Niger, and the largest flowing into the Indian Ocean from the African continent. The river originates in northwest Zambia (11.370°S, 024.308°E, 1450 m a.s.l.), and flows south-east over 3000 km before it discharges into the Indian Ocean in Mozambique (Fig. 1). Based on distinct geomorphological characteristics, the Zambezi River is divided into three major segments: (i) the Upper Zambezi from the headwaters to the Victoria Falls, (ii) the Middle Zambezi, from the Victoria Falls to the edge of the Mozambique coastal plain (below Cahora Bassa Gorge), and (iii) the Lower Zambezi, the stretch traversing the coastal plain down to the Indian Ocean (Wellington, 1955; Moor et al., 2007). The upper reaches of the river are incised into Upper Precambrian crystalline basement rocks composed of metamorphosed sediments including shale, dolomite and quartzite. Further downstream, the Zambezi widens into the Barotse Floodplain, a very low gradient stretch that traverses unconsolidated sands, known as the Kalahari Sand. Downstream of the Barotse Floodplains, the gradient of the Zambezi steepens and the river begins to incise into Karoo-age basalts and sediments (sandstone, shale, limestone) that form the sub Kalahari bedrock, creating a series of rapids and falls with the Victoria Falls (world's second largest: 1708 m width, 108 m height) marking the edge of the Upper Zambezi stretch (Moor et al., 2007). The Middle Zambezi is characterized by a

markedly steeper gradient than the section above the falls with an initial turbulent course through a series of narrow zigzag gorges and rapids before the river widens into the broad basins of the Kariba and Cahora Bassa reservoirs. Karoo-age basalts and sediments and subordinate Precambrian crystalline basement rocks (gneiss and granite) constitute the bedrock over most of this stretch of the river (Moor et al., 2007). Downstream of the Cahora Bassa Reservoir, the river flows through one last gorge (the Cahora Bassa Gorge) before entering a more calm and broader stretch of the Lower Zambezi. Traversing the Cretaceous and Tertiary sedimentary cover of the Mozambique coastal plain, the lower reaches of the river forms a large, 100-km long floodplain-delta system of oxbows, swamps, and multichannel meanders.

Along its course, the Zambezi River collects water from many tributaries from both left and right banks (Fig. 1) which contribute with different proportion to the annual average discharge, which ranges between 3424 and 4134 $m^3 s^{-1}$ (Beilfuss and dos Santos, 2001; World Bank, 2010). With a mean discharge of 320 $m^3 s^{-1}$, the Kafue River is the major tributary of the Zambezi. The river originates in northwest Zambia, flows south, south-east for over 1550 km and joins the Zambezi River ~70 km downstream of the Kariba Dam. Its drainage basin of over 156000 km^2 which lies entirely within Zambia is home to almost half of the country's population, and has a large concentration of mining, industrial and agricultural activities.

There are two major impoundments along the Zambezi River. The Kariba Reservoir, completed in 1959 between Zambia and Zimbabwe, about 170 km downstream of the Victoria Falls (Fig. 1), is the world's largest reservoir by volume (volume: 157 km^3; area: 5364 km^2, Kunz et al., 2011a). Completed in 1974 in Mozambique, about 300 km downstream of the Kariba Dam (Fig. 1), the Cahora Bassa Reservoir is the fourth largest reservoir in Africa (volume: 52 km^3; area: 2675 km^2, Beilfuss and dos Santos, 2001). Contemporaneous with the construction of the Cahora Bassa Dam, two smaller reservoirs have been created on the Kafue

River: (i) the Kafue Gorge Reservoir (volume: ~1 km^3; area: 13 km^2) completed in 1972 about 75 km upstream from the confluence with the Zambezi with the purpose of power generation, and (ii) the Itezhi Tezhi Reservoir (volume: ~6 km^3, area: 365 km^2) completed in 1978 about 270 km upstream (Fig. 1), which serves as storage reservoir to ensure constant water supply for the Kafue Gorge dam.

The climate of the Zambezi basin, classified as humid subtropical, is generally characterized by two main seasons: the rainy season from October/November to April/May, and the dry season from May/June to September/October (Fig. 2). Annual rainfall across the river basin (mean 940 mm for the entire catchment) varies with latitude from about 400 to 500 mm in the extreme south and southwest part of the basin to more than 1400 mm in the northern part and around Lake Malawi (Chenje, 2000). Up to 95% of the annual rainfall in the basin occurs during the rainy season while irregular and sporadic rainfall events during the dry period contribute generally up to 5%. Driven by seasonality in rainfall patterns, the hydrological cycle of the Zambezi River has a bi-modal distribution, characterized by a single main peak flood with maximum discharge occurring typically in April/May and minimum in November. An example of the seasonality and the disturbance of the natural flow pattern associated with river damming is illustrated in Fig. 2, based on daily discharge data measured at 4 sites in the basin between January 2012 and January 2014.

Almost 75% of the basin is covered by forest and bush. Cropped land (with mostly rain-fed agriculture) covers up to 13%, and grassland cover about 8% of the land area (SADC et al., 2012). Wetlands, comprising swamps, marshes and seasonally inundated floodplains, cover more than 5% of the total basin area (SADC et al., 2012, McCartney et al., 2013). Important wetlands in the basin include the Lungue Bungo Swamps, Luena Flats, Barotse Floodplain, Kafue Flats and Luangwa Floodplain in Zambia, the Mid-Zambezi Valley and

168 Mano Pools in Zimbabwe, the Shire Marshes in Malawi and the Lower Zambezi and Zambezi
169 Delta in Mozambique (McCartney et al., 2013).

170 In 1998, the population in the basin was estimated at 31.7 million (one-third of the
171 total population of the eight basin countries), out of which more than 85% lives in Malawi,
172 Zambia and Zimbabwe. Ten years later (2008) the population reached over 40 million and it
173 is predicted to achieve 51.2 million by 2025 (SADC et al., 2012). This predicted increase in
174 population, alongside with ongoing economical development in the region and new
175 hydropower projects is expected to exert further pressure on the aquatic environment and
176 natural water resources of the basin.

177

178 **2.2 Sampling strategy and analytical techniques**

179 Sampling was conducted during two consecutive years and over two climatic seasons: wet
180 season (1 February to 5 May) 2012, wet season (6 January to 21 March) 2013, and dry season
181 (15 October to 28 November) 2013 (Fig. 2). Up to 56 sites were visited each campaign,
182 depending on logistics and accessibility. Sampling sites (chosen at 100-150 km apart) were
183 located as follows: 26 along the Zambezi mainstream (including 3 sites on the Kariba and 3
184 on the Cahora Bassa reservoirs), 2 on the Kabompo, 13 along the Kafue (including 3 on the
185 Itezhi Tezhi Reservoir), 3 on the Lunga (main tributary of the Kafue), 5 along the Luangwa, 2
186 on the Lunsemfwa (main tributary of the Luangwa), one on the Mazoe and one on the Shire
187 River (Fig. 1). In situ measurements and water sampling was performed, whenever possible,
188 from boats or dugout canoes in the middle of the river at ~0.5 m below the water surface.
189 However, in the absence of boats/canoes, sampling was carried out either from bridges or
190 directly from the shore and as much as possible away from the shoreline.

191 At each location, *in situ* measurements of water temperature, dissolved oxygen (DO),
192 conductivity and pH were performed with a YSI ProPlus multimeter probe. The pH and DO

probes were calibrated each time before the measurement using United States National Bureau of Standards buffer solutions of 4 and 7, and water saturated air. The partial pressure of CO_2 (pCO_2) in the water was measured *in situ* with a PP-Systems EGM-4 non-dispersive, infrared gas analyzer (calibrated before each field cruise with a certified gas standard with a mixing ratio of 1017 ppm) using both a Liqui-Cel MiniModule membrane contactor equilibrator and a headspace technique. For the first method, the water pumped from ~0.5 m depth, was circulated through the exchanger at a constant flow rate of ~0.35 L min^{-1}, and the gases were continuously re-circulated in a closed loop into the EGM-4 for instantaneous measurements of pCO_2. At a flow rate of 0.35 L min^{-1}, the half-equilibration time of CO_2 in the MiniModule is 4–5 sec. For the headspace technique, 30 mL of water, collected (under the water) into five 60-mL polypropylene syringes was mixed with 30 mL air of known CO_2 concentration and gently shaken for 5 minutes allowing the equilibration of the two phases. The headspace volume (30 mL) was then transferred into a new syringe and directly injected into the EGM-4 analyzer. Water pCO_2 was calculated from the ratio between the air and water volumes using the gas solubility at sampling temperature. Comparison between and the syringe-headspace and membrane equilibrator techniques gave consistent results with slope not significantly different from unity (1.09), r^2=0.992, $p<0.0001$, n=83, in the 140-14000 ppm range (Abril et al., 2015).

CO_2 fluxes to the atmosphere were measured using a custom-designed floating chamber (Polyvinyl chloride cylinder of 38 cm internal diameter, 15 cm active height, plus 7 cm skirt under the air-water interface) connected at the top-most through 2 rubber-polymer tubes (Ø=0.45 cm) to a non-dispersive infrared analyzer (PP-System, EGM-4). Starting at atmospheric concentration (and pressure), the air inside the chamber (17 L volume) was circulated in a closed loop and analyzed for CO_2 with readings every ½ min over a 30 min period. Temperature inside the chamber was monitored continuously with a VWR 4039

Waterproof Thermometer (accuracy ±1°C) and further used in the flux calculation. For the determination of CH_4 fluxes, a 60-mL syringe, fitted on a third tube with a two-way valve was filled with 30 mL air from inside the chamber at 0, 5, 10, 20 and 30 min interval. Transferred immediately into a 50-mL serum vial, pre-filled with saturated saline solution, samples were stored in upside-down position until analyzed in the laboratory by gas chromatography (GC) (see below). Fluxes to atmosphere were estimated from the change in concentrations using the following equation:

$$F = [(s \times V)/(mV \times S)] \times f \quad (1)$$

where: F is the flux in µmol m^{-2} d^{-1}; s is the slope in µatm min^{-1}; V is the volume of the chamber in liters (L); mV (molar volume) is the volume of one mole of gas in L atm mol^{-1}; S is the surface area of the floating chamber over the water in m^2; and f is the conversion factor from minutes to days (1d = 1440 min) (see Teodoru et al., 2010). Measurements were performed on drift, with the chamber flowing alongside the current. Whenever possible, flux chamber measurements were performed on both static and drift-mode with constant records of water velocity (relative to the chamber for static mode) and drift velocity to account for the enhanced gas exchange coefficient due to local-induced turbulence by the chamber itself. At each location, before and after chamber measurements, additional ambient air pCO_2 was measured by injecting air samples into the EGM-4 analyzer, while air temperature, barometric pressure, humidity and wind speed were measured at ~1 m above the water surface using a hand-held anemometer (Kestrel 4000, accuracy 3%). Measurement precision of pCO_2 with the EGM-4 was ±1%, and the stability/drift of the instrument (checked after each cruise), was always less than 2%.

Samples for dissolved CH_4, N_2O and the stable isotope composition of DIC ($\delta^{13}C_{DIC}$) were collected in 50 mL serum bottles (for CH_4 and N_2O) and 12 mL exetainer vials (for $\delta^{13}C_{DIC}$) filled from the Niskin bottle (allowing water to overflow), poisoned with $HgCl_2$, and capped without headspace. Concentrations of CH_4 and N_2O were determined by the headspace equilibration technique (20 mL N_2 headspace in 50 mL serum bottles) and measured by GC (Weiss, 1981) with flame ionization detection (GC-FID) and electron capture detection (GC-ECD) with a SRI 8610C GC-FID-ECD calibrated with CH_4:CO_2:N_2O:N_2 mixtures (Air Liquide Belgium) of 1, 10 and 30 ppm CH_4 and of 0.2, 2.0 and 6.0 ppm N_2O, and using the solubility coefficients of Yamamoto et al. (1976) for CH_4 and Weiss and Price (1980) for N_2O. The overall precision of measurements was ±4% for CH_4 and ±3% for N_2O. For the analysis of $\delta^{13}C_{DIC}$, a 2 ml helium (He) headspace was created, and H_3PO_4 was added to convert all DIC species to CO_2. After overnight equilibration, part of the headspace was injected into the He stream of an elemental analyzer – isotope ratio mass spectrometer (EA-IRMS, ThermoFinnigan Flash HT and ThermoFinnigan DeltaV Advantage) for $\delta^{13}C$ measurements. The obtained $\delta^{13}C$ data were corrected for the isotopic equilibration between gaseous and dissolved CO_2 as described in Gillikin and Bouillon (2007), and measurements were calibrated with certified reference materials LSVEC and either NBS-19 or IAEA-CO-1.

For total alkalinity (TA), 80 mL of water samples were filtered on 0.2 µm polyethersulfone syringe filters (Sartorius, 16532-Q) and analyzed by automated electro-titration on 50 mL samples with 0.1 mol L^{-1} HCl as titrant (reproducibility was typically better than ±3 µmol L^{-1} based on replicate analyses). DIC concentrations were computed from TA, water temperature and pCO_2 measurements using thermodynamic constants of Millero (1979) as implemented in the CO2SYS software (Lewis and Wallace, 1998). Using an estimated error for pCO_2 measurements of ±1%, ±3 µM for TA, and ±0.1°C for temperature, the

propagated error for DIC is ±5%. The concentrations of calcium (Ca), magnesium (Mg), and dissolved silica (DSi) were measured using inductively coupled plasma-atomic emission spectroscopy (Iris Advantage, Thermo Jarrel-Ash). Pelagic community respiration (R) rates were determined by quantifying the decrease in DO (with the optical DO probe YSI-ODO) using triplicate 60 mL Winkler bottles, incubated in a dark coolbox filled with water (to retain ambient temperature) for approximately 24 h. A respiratory molar oxidation ratio of 1.3 O_2:C was used as the conversion rate from oxygen measurements into C (Richardson et al., 2013). Particulate primary production (P) rates in surface waters (i.e. not depth-integrated rates) were quantified in duplicate by determining the uptake of DIC after short-term (2–3 h) *in situ* incubations of river water during the day using 1 L polycarbonate bottles spiked with ^{13}C-labelled sodium bicarbonate ($NaH^{13}CO_3$). A subsample of the spiked water was sampled to measure the degree of ^{13}C-enrichment in the DIC pool. Samples for analysis of $\delta^{13}C_{POC}$ were obtained at the start (natural abundance values) and at the end of the incubation by filtering a known volume of surface water on pre-combusted (overnight at 450 °C) 25mm GF/F filters (0.7 µm). Filters were decarbonated with HCl fumes for 4 h, re-dried and then packed into Ag cups. Particulate organic carbon (POC) and $\delta^{13}C_{POC}$ were determined on a Thermo elemental analyzer – isotope ratio mass spectrometer (EA-IRMS) system (Flash HT with Delta V Advantage), using the thermal conductivity detector signal of the EA to quantify POC and by monitoring m/z 44, 45 and 46 on the IRMS. Quantification and calibration of δ^{13}C data were performed with IAEA-C6 and acetanilide that was calibrated against international standards. Reproducibility of $\delta^{13}C_{POC}$ measurements was typically better than 0.2‰. Calculations to quantify the P rates were made as described by Dauchez et al. (1995). The R and P data here (in µmol C L^{-1} h^{-1}) refer only to surface water (~0.5m deep) measurements and not to depth-integrated values.

3 Results and Discussion

3.1 Temporal and spatial variability of pCO_2

pCO_2 along the Zambezi River was highly variable, both spatially and temporally. Riverine pCO_2 was generally higher during wet seasons compared to the dry season (Fig. 3a). Lowest riverine values (i.e. excluding reservoirs) during wet seasons 2012 and 2013 of 640 and 660 ppm, respectively, were found immediately below the Victoria Falls, while highest concentrations were always recorded downstream of the Barotse Floodplains (7650 and 10350 ppm, respectively) and downstream of the confluence with the Shire River in Mozambique (8180 and 12200 ppm, respectively) (Fig. 3a). During the dry season of 2013, the lowest concentration (300 ppm, i.e. below atmospheric equilibrium) was measured at ZBZ.6, while highest pCO_2 was found at the river source and immediately below the Kariba Dam (2550 and 2600 ppm, respectively, Fig. 3a). Mean pCO_2 for the entire river (i.e. excluding reservoirs) was 2475 ppm and 3730 ppm, respectively, during the wet season of 2012 and 2013, but only 1150 ppm (measurements up to ZBZ.13 only) during the dry season of 2013. Despite relatively large interannual variability (paired *t*-test significantly different, $p<0.025$, $n=15$), but low seasonality ($p<0.09$, $n=8$), pCO_2 along the Zambezi followed the same longitudinal pattern (slightly different during dry season) (Fig. 3a). The pCO_2 was always below atmospheric equilibrium in the surface water of the two major reservoirs (mean for all campaigns: 267 ppm for Kariba and 219 ppm for Cahora Bassa) with no distinct interannual variability or seasonality (Fig. 3a).

Large variability of riverine pCO_2 was also observed for the Kafue River (Fig. 3b). Excluding reservoir values, pCO_2 along the Kafue River varied between 905 and 1145 ppm during the wet season of 2012 and 2013, respectively (both recorded at KAF. 6 located immediately below the Itezhi Tezhi Dam), up to 9985 and 11745 ppm, respectively (both measured at KAF.8 in the Kafue Flats). Concentrations were consistently lower during the dry

317 season 2013, ranging from 330 ppm at KAF.4 (below the Lukanga Swamps) up to 6650 ppm
318 at the end of the Kafue Flats (KAF.9) (Fig. 3b). With mean pCO_2 for the entire river of 3805
319 and 4748 ppm, respectively (without the Ithezhi Tezhi Reservoir), values in the Kafue were
320 significantly different during the two wet season campaigns (paired t- test, $p<0.009$, $n=9$) as
321 well as during 2013 dry season compared to 2013 wet season ($p<0.026$, $n=7$, mean 2770
322 ppm). pCO_2 in the surface water of the Itezhi Tezhi Reservoir was always above atmospheric
323 concentration during both wet seasons (mean 1130 ppm in 2012 and 1554 ppm in 2013),
324 showing a decreasing pattern with increasing the distance from the river inflow. The only
325 measurement during dry season 2013 in the middle of the reservoir (ITT.2) indicated strong
326 CO_2 undersaturated conditions (165 ppm). As observed for the Zambezi River, the variability
327 of pCO_2 along the Kafue River followed a similar pattern during each campaign.

328 Overall, there was a relatively good ($r^2=0.78$), negative correlation between CO_2
329 (µmol L^{-1}) and DO concentration (µmol L^{-1}) for all sampled rivers, tributaries and reservoirs,
330 and during all campaigns (Fig. 3c) with mostly reservoir samples characterized by high DO
331 and low CO_2 content while hypoxic conditions associated with high CO_2 values were
332 characteristic for the Shire River, and several stations on the Zambezi and the Kafue Rivers
333 (mostly downstream of floodplains). The slope of this relationship of 0.79±0.04, could
334 provide an estimate of the respiratory quotient (RQ) defined as the molar ratio of O_2
335 consumed to CO_2 produced by respiration. The RQ value is in theory equal to 1 for the
336 oxidation of glucose, but higher than 1 for more complex and reduced organic molecules
337 containing nitrogen and phosphorous, such as lipids and proteins, or lower than 1 for highly
338 oxidized and oxygen-rich molecules (e.g. pyruvic, citric, tartaric, and oxalic acids) (Berggren
339 et al., 2012). The value we computed is lower than the RQ value of 1.3 established in a
340 temperate stream with a catchment dominated by pastures (Richardson et al., 2013), but close
341 to the one recently proposed for bacterial respiration in boreal lakes of 0.83 (Berggren et al.,

342 2012). Berggren et al. (2012) attribute this low RQ to the bacterial degradation of highly
343 oxidized molecules such as organic acids, likely to be also abundant at our sampling sites
344 (Lambert et al., 2015).

345 With an overall mean of 2639 ppm over the entire sampled period (both wet and dry),
346 pCO_2 of the Zambezi River was 45% lower than mean pCO_2 of the Kafue River (mean 3852
347 ppm) (Fig. 4d). All other tributaries displayed also CO_2 supersaturated conditions with respect
348 to atmospheric equilibrium with mean values ranging from as low as 955 and 1402 ppm in the
349 Mazoe and the Luangwa rivers and up to 13351 ppm in the Shire River (Fig. 4d). While mean
350 values of the two large reservoirs on the Zambezi River indicate undersaturated CO_2
351 conditions, overall mean pCO_2 of the much smaller Itezhi Tezhi Reservoir on the Kafue River
352 of 1174 ppm was well above atmospheric equilibrium (Fig. 4d).

353

354 **3.2 Temporal and spatial variability of CH_4**

355 CH_4 along the Zambezi also showed a relatively large spatial heterogeneity, but low temporal
356 variability (Fig. 4a). Lowest CH_4 concentrations during the two wet season campaigns (2012
357 and 2013) of 7 and 13 nmol L^{-1}, respectively, were both recorded at station ZBZ.9
358 immediately below the Victoria Falls. Highest value of the wet season 2012 campaign of
359 2,394 nmol L^{-1} was measured at ZBZ.17 while highest CH_4 concentration of the wet season
360 2013 of 12127 nmol L^{-1} was recorded at station ZBZ.5, downstream of the Barotse Floodplain
361 (Fig. 4a). Mean value of the 2012 wet season campaign of 623 nmol L^{-1} was 2 fold lower than
362 mean CH_4 of the 2013 wet season (1,216 nmol L^{-1} driven by the extremely high value at
363 station ZBZ.5), but median (348 and 274 nmol L^{-1} for 2012 and 2013 wet seasons,
364 respectively) and statistical analyses (paired *t*-test, $p>0.516$, $n=15$) suggest no significant
365 interannual variability. In the absence of comparative measurements at station ZBZ.9 below
366 the Victoria Falls, lowest CH_4 concentration along the Zambezi during dry season 2013

campaign of 25 nmol L^{-1} was recorded at ZBZ.10 in the Kariba Gorge (4 km downstream of the Kariba Dam), whereas maximum value of 874 nmol L^{-1} was measured at ZBZ.5, downstream the Barotse Floodplains (Fig. 4a). Although mean CH_4 of the dry season 2013 of 361 nmol L^{-1} was much lower than the equivalent mean of the wet season 2013 campaign, its median value of 305 nmol L^{-1} and the paired t-test ($p>0.368$, $n=8$) indicate little CH_4 seasonality along the Zambezi River. CH_4 concentrations in the surface water of the two reservoirs on the Zambezi were generally lower compared to the riverine values, and consistently below levels measured at the stations immediately downstream both dams (Fig. 4a). Concentrations in the Kariba were higher during wet season 2012 (mean 149 nmol L^{-1}) compared to the wet season 2013 (mean 28 nmol L^{-1}) but opposite in the Cahora Bassa (mean 54 and 78 nmol L^{-1}, respectively). The only CH_4 measurement in the Kariba Reservoir during dry season 2013 reached 19 nmol L^{-1} (Fig. 4a).

Relatively low temporal variability of CH_4 (both interannual and seasonal) was also observed along the Kafue River (Fig. 4b), where concentrations varied from minimum 30, 100, and 92 nmol L^{-1} during wet seasons 2012 and 2013, and the dry season 2013, respectively (all recorded at KAF.6, immediately below the Itezhi Tezhi Dam) to maximum 992 nmol L^{-1} in the Kafue Flats (KAF.8) during 2012 wet season, and 550 and 898 nmol L^{-1}, respectively, at the lower edge of the flats (KAF.9) during 2013, both wet and dry seasons. With mean CH_4 values of 405, 329, and 416 nmol L^{-1} (or median 298, 302, and 274 nmol L^{-1}) for the wet seasons 2012 and 2013, and the dry season 2013, respectively, CH_4 concentrations along the Kafue were not statistically different during the wet season 2012 compared to the wet season 2013 (paired *t*-test, $p>0.541$, $n=9$), nor during 2013 wet and dry seasons ($p>0.543$, $n=7$). CH_4 concentrations in the surface water of the Ithezhi Tezhi Reservoir were generally lower than riverine values, ranging between 37 and 89 nmol L^{-1} (mean 62 nmol L^{-1}) during wet season 2012, and 22 and 51 nmol L^{-1} (mean 40 nmol L^{-1}) during wet season 2013 (Fig.

392 4b). The only CH_4 measurement during 2013 dry season in the Itezhi Tezhi Reservoir (ITT.2)
393 reached 71 nmol L^{-1}.

394 There was an overall positive, albeit weak (r^2=0.186, n=106) correlation between CH_4
395 and pCO_2 (log-log scale) for all rivers, tributaries and reservoirs, and all campaigns, with
396 values at the lowest end mostly characteristic for the Kariba and Cahora Bassa reservoirs, and
397 higher end occupied by the Shire River and several stations on the Zambezi and Kafue rivers
398 located in or downstream of major floodplains/wetlands (Fig. 4c). With an arithmetic average
399 value (all samples) of 769 nmol L^{-1} for the entire sampled period, CH_4 of the Zambezi River
400 was twice as high as the equivalent average CH_4 concentration of the Kafue River (mean 381
401 nmol L^{-1}) (Fig. 4d). With the exception of the Shire River which displayed extremely high
402 concentration (mean 19328 nmol L^{-1} based on only 2 measurements), all other tributaries of
403 the Zambezi River had similar mean CH_4 level ranging from 200 nmol L^{-1} in the highly turbid
404 Luangwa River up to 514 nmol L^{-1} in the Lunsemfwa River (tributary of Luangwa) (Fig. 4d).
405 CH_4 concentrations in the surface water of all three reservoirs were comparable (mean 87, 66
406 and 54 nmol L^{-1} for Kariba, Cahora Bassa and Itezhi Tezhi, respectively) and generally lower
407 then riverine values (Fig. 4d). With the exception of the Itezhi Tezhi, CH_4 values measured at
408 stations immediately below both Kariba and Cahora Bassa dams were substantially higher
409 compared to levels characterizing the surface water of the two reservoirs
410
411 **3.3 Temporal and spatial variability of N_2O**
412
413 N_2O in the Zambezi River was also characterized by high spatial variability. During both
414 2012 and 2013 wet season campaigns, N_2O along the Zambezi ranged from 4.1 nmol L^{-1} at
415 ZBZ.5 (downstream of the Barotse Floodplain) and 2.9 nmol L^{-1} at ZBZ.18 (downstream the
416 confluence with the Shire River) up to 8.5 and 8.0 nmol L^{-1}, respectively, both at ZBZ.11,

downstream of the Kariba Dam (Fig. 5a). Higher overall concentrations but lower spatial variability was recorded during the dry season 2013, when concentrations ranged between 7.9 nmol L^{-1} at ZBZ.13 (upstream of the Cahora Bassa Reservoir) and 11.4 nmol L^{-1} at ZBZ.10 (downstream of the Kariba Dam) (Fig. 5a). Statistical analyses of N_2O concentrations of the two wet season campaigns (mean 6.7, and 6.1 nmol L^{-1} for 2012 and 2013, respectively) and the dry season 2013 (mean 8.8 nmol L^{-1}) suggest low interannual variability (paired *t*-test, $p>0.142$, n=15) but strong N_2O seasonality (paired *t*-test, $p<0.0004$, n=8) along the Zambezi River mainstem. The only measurement during the dry season 2013 in the surface water of the Kariba reservoir suggest that N_2O was also higher (mean 8.6 nmol L^{-1}) compared to values of wet seasons 2012 and 2013 (mean 6.3 and 6.5 nmol L^{-1}, respectively). The same high spatial heterogeneity and low N_2O interannual variability was observed along the Kafue River, where values of the 2012 and 2013 wet seasons (mean 5.9 nmol L^{-1} and 5.7 nmol L^{-1}, respectively) were not statistically different (paired *t*-test, $p>0.549$, n=9). It is worth noting that both minimum N_2O values of the two consecutive wet season campaigns (3.9 and 3.0 nmol L^{-1}, respectively) were recorded at station KAF.8 in the Kafue Flats. Consistently higher and ranging from 7.0 nmol L^{-1} in the Kafue Flats to 10.3 nmol L^{-1} at the headwater station (KAF.1), N_2O during the dry season 2013 (mean 8.4 nmol L^{-1}) was significantly higher (paired *t*-test, $p<0.001$, n=7) compared to the 2013 wet season. N_2O in the surface water of the Itezhi Tezhi Reservoir were similar during both wet season campaigns (mean 6.8 and 6.5 nmol L^{-1}, respectively) and slightly higher than riverine values. The only one N_2O measurement in the Itezhi Tezhi during dry season 2013 (at ITT.2) reached 7.8 nmol L^{-1} (Fig. 5b).

There was an overall good ($r^2=0.48$) and negative correlation between N_2O and pCO_2 (Fig. 5c), with high N_2O concentrations and low pCO_2 mostly characteristic for reservoirs and riverine stations downstream of dams, while low N_2O and high pCO_2 were characteristic for

442 the Shire River and stations on the Zambezi and Kafue downstream of floodplains. There was
443 no correlation between N_2O and NH_4^+ nor NO_3^-, while a positive relation with %DO was only
444 found during wet seasons (data not shown). Despite seasonal and longitudinal variations,
445 mean N_2O values were relatively similar among tributaries with little variability (means from
446 6.2 nmol L^{-1} for the Lunga to 7.5 nmol L^{-1} for the Lunsemfwa), with the exception of the
447 Shire River characterized by distinct lower value (mean 2.7 nmol L^{-1}) (Fig. 5d). N_2O in the
448 surface water of the Kariba and the Cahora Bassa reservoirs (mean 6.8 and 7.3 nmol L^{-1},
449 respectively) were close to riverine values (Fig. 5d).
450
451 **3.4 Patterns in GHG dynamics along the river continuum**
452 As shown above, dissolved GHG concentrations along the Zambezi and the Kafue rivers
453 display large spatial heterogeneity. Yet, concentrations followed similar longitudinal patterns
454 during both consecutive wet season campaigns and only slightly different during dry season,
455 which can be attributed to the connectivity between river and floodplains/wetlands, the input
456 from major tributaries, and the presence of natural or anthropogenic barriers (waterfalls/rapids
457 and reservoirs) along the aquatic continuum. We will examine these patterns in detail, using
458 the example of pCO_2 during the 2012 wet season campaign since this represents the most
459 complete dataset (Fig. 3a).
460 Starting at an initial 1055 ppm at the Zambezi source (ZBZ.1), pCO_2 increased
461 downstream to about 2450 ppm at ZBZ.2 as the river traverses a low gradient area, receiving
462 water from the Chifumage and Luena tributaries which drain large floodplains in SE Angola.
463 After a small decrease to 1970 ppm downstream of the confluence with the Kabompo River
464 (ZBZ.3), pCO_2 increased sharply to over 7650 ppm at ZBZ.5 (ZBZ.4 was not sampled during
465 wet season) as the river exchanges waters with the Barotse Floodplains. This high CO_2 load,
466 associated with low pH (6.97) and %DO (47%) (Supplementary material, Table S1), was

rapidly outgassed downstream due to a sharper gradient of this river sector which forms several rapids and the 14-m high Nygone Falls, reaching only 1980 ppm at ZBZ.6. Further downstream, pCO_2 peaked again (>6300 ppm at ZBZ.7) as the river passes though the Caprivi-Chobe Swamps, but dropped quickly down to 2500 ppm upstream of the Victoria Falls (ZBZ.8) due to the further steepening of the river gradient and the enhanced turbulent flow over the Mambova and the Katombora Rapids. As the river plunged down over 100 m height of the Victoria Falls, there was an instant and almost complete CO_2 outgassing, with river waters approaching atmospheric equilibrium at the base of the fall (642 ppm at ZBZ.9). Downstream of the Victoria Falls, the river experiences a turbulent flow through the narrow, 100-km long Batoka Gorge and the Chimba Rapids, and CO_2 is expected to decrease further approaching atmospheric concentrations at the inflow of the Kariba Reservoir. These CO_2-depleted inflow waters combined with CO_2 uptake by primary production (mean P ~16.6 µmol C L^{-1} h^{-1}) could be put forward to explain the CO_2 under-saturated conditions encountered in the surface waters of the Kariba Reservoirs throughout all campaigns (Fig. 3a). In contrast to the CO_2 undersaturated (and warmer, DO saturated) epilimnetic conditions of the Kariba Reservoir, much higher pCO_2 (>2000 ppm, accompanied by colder water and undersaturated DO conditions) measured 70 km downstream of the Kariba Dam (at ZBZ. 11) suggests the discharge at the dam of hypolimnetic, low DO and CO_2-loaded waters, formed as a result of thermal stratification of the water column of the reservoir (Kunz et al., 2011a). Even though no major tributaries or other point sources (i.e. wetlands) exist along this 70-km stretch, the potential contribution of lateral sources to the pCO_2 measured at ZBZ.11 cannot be totally ruled out. However, measurements during 2013 dry campaign showed a constant decrease in pCO_2 (and an increase in %DO and water temperature) between the intermediate point ZBZ.10 (located 17 km downstream the dam) and ZBZ.11 from 2600 ppm (65% DO and 24.1°C) to 1600 ppm (82% DO and 24.3°C), respectively. This higher upstream pCO_2

492 level at ZBZ.10 and the steady downstream decrease (accompanied by increase in %DO and
493 water temperature) support the idea of hypolimnetic water discharge with high pCO_2 which,
494 even if partially decreased due to CO_2 efflux to the atmosphere , it is still reflected in the
495 pCO_2 measured 70 km downstream at ZBZ.11. Low re-aeration rates with hypoxic conditions
496 caused by periodically hypolimnetic water discharge have been previously described to last
497 for more than 100 km downstream the Itezhi Tezhi dam (Kunz et al., 2013). A simple
498 calculation based on mass balance approach which assumes no additional lateral CO_2 source
499 along this 70 km stretch, and uses the CO_2 concentrations and fluxes measured at ZBZ.11
500 during all three sampling campaigns together with the daily discharge rates at Kariba dam
501 suggest that pCO_2 at the outlet of the reservoir would vary between 3500 and 4600 ppm. Even
502 these estimated figures may be in fact slightly higher since the (low) fluxes at ZBZ.11 are not
503 representative for the entire 70 km stretch (especially for the narrow and steep Kariba Gorge
504 section), they are still substantially lower compared to pCO_2 ranges measured in the
505 hypolimnion of several tropical reservoirs (Guérin et al., 2006).

506 Riverine pCO_2 decreased further downstream of site ZBZ.11 through CO_2 efflux to the
507 atmosphere, favored by the substantial broadening of the river sector, reaching 1230 ppm at
508 ZBZ.12 and 890 ppm at ZBZ.13. pCO_2 in the surface water of the Cahora Bassa reservoir was
509 below atmospheric equilibrium (168 and 342 ppm) and generally similar to those measured in
510 the Kariba. As in the case of Kariba, pCO_2 measured 40 km downstream of the Cahora Bassa
511 dam (at ZBZ.14) of 1800 ppm (and 340 nmol L^{-1} CH_4 compared to ~50 nmol L^{-1} in the
512 surface water of the reservoir) suggests the discharge of hypolimnetic water through the
513 bottom intake with high CO_2 (and CH_4) content. pCO_2 decreased further downstream the dam
514 due to the turbulent flow throughout the narrow Cahora Bassa Gorge and the broadening of
515 the river section towards the coastal plains, reaching 815 ppm and 560 ppm at ZBZ.15 and
516 ZBZ.16, respectively. Further downstream, pCO_2 increased up to 1205 ppm (at ZBZ.17),

most probably influenced by the wide riparian wetlands/marshes along the river banks, and increased further downstream to over 8180 ppm at ZBZ.17 as the Zambezi River receives waters from the highly CO_2 oversaturated Shire River (12700 ppm CO_2, 17.3% DO) that drains a stagnant water complex of swamp/marshes (known as the Elephant Marsh). This high CO_2 load was slowly exchanged with the atmosphere towards the delta with river pCO_2 reaching 1790 ppm at ZBZ.19 and 1610 ppm at ZBZ.20 close to the river mouth (Fig. 3a).

This longitudinal pattern of pCO_2 along the Zambezi River described above was closely repeated during the second wet season campaign (Fig. 3a). Despite the overall lower values during the dry season 2013, pCO_2 followed also a relatively similar pattern reflecting also the influence of the Barotse floodplains (although less pronounced), the quick CO_2 outgassing downstream due to the presence of several rapids and the Nygone Falls as well as the influence of the Chobe swamps (Fig. 3a). The only obvious difference relative to the wet seasons occurred in the Zambezi headwaters when pCO_2 decreased substantially between the source station ZBZ.1 and ZBZ.2 compared to the increased pattern observed during both wet seasons. This could be potentially explained by the reduction of lateral input load as a result of loss of connectivity between the river and the riparian wetlands associated with lower water level during dry season.

Similar longitudinal patterns, reflecting the influence of wetlands, reservoirs, and waterfalls/rapids along the Zambezi mainstem were also observed for CH_4 (Fig. 4a) as well as for N_2O, with the latter showing a mirror image of the patterns in pCO_2 (Fig. 5a). The positive relationship between CH_4 and CO_2 suggest that both are largely controlled by organic matter degradation processes. The negative relationship between N_2O and pCO_2 and the positive relationship between N_2O and %DO suggest, on the other hand, that N_2O is removed by denitrification in the sediments. Low N_2O levels have been also observed in the Amazon floodplains (Richey et al., 1988) and in the hypolimnion of anoxic lakes (Mengis et al., 1997).

The influence of wetlands/floodplains and reservoirs on the dynamics of pCO_2 can be also seen along the Kafue River (Fig. 3b) where a steady increase in pCO_2 values was recorded during both wet seasons (2012 and 2013) at station KAF.4 below the Lukanga swamps as well as in-, and downstream of the Kafue Flats (KAF.7, KAF.8, KAF.9) (Fig. 3b). The different pattern (decrease instead of increase) during the dry season 2013 for the upper Kafue (upstream of the Itezhi Tezhi Reservoir) can be explained by the loss of connectivity between river mainstem and the swamps. Low water levels during dry season 2013 which partially exposed the river bedrock along this stretch enhanced the turbulent flow (and subsequently the gas exchange coefficient) as suggested by oversaturated DO value (143%), lowering the pCO_2 level close to atmospheric equilibrium. In the absence of an important lateral CO_2 source, photosynthetic CO_2 uptake by primary production higher than in the Kariba reservoir (P ~21.8 µmol C L^{-1} h^{-1}) should have further reduced the CO_2 down to undersaturated conditions. The peculiar situation downstream of the Itezhi Tezhi Reservoir where riverine pCO_2 showed an increase in-, and downstream of the Kafue Flats also during 2013 dry season campaign can be explained by the specific hydrology of the flats altered by the operation of the two bordering dams. The completion of the Kafue Gorge Dam in 1972 led to an average rise in water table of over 2 m in the lower Kafue Flats which created a permanently flooded area of over 800 km^2 (McCartney and Houghton-Carr, 1998). Completed in 1978 with the purpose of upstream storage in order to ensure constant water supply for the Kafue Gorge Dam, the Itezhi Tezhi further altered the hydrology of the Kafue Flats. Triggered by rising energy demands, flows at the Itezhi Tezhi Dam have increased substantially during dry seasons while flood peaks have partly been delayed and attenuated, changing the timing and extent of flooding in the Kafue Flats (Mumba and Thompson, 2005). This hydrological alteration due to river damming responsible for the creation of a permanent flooded area within the Kafue Flats which constantly exchanges water with the Kafue River

mainstem could explain the observed high riverine pCO_2 levels there encountered also during the dry season 2013 (Fig. 3b). In contrast to the Zambezi River where riverine CO_2 concentrations downstream both dams were significantly higher compared to those in the surface water reservoirs, pCO_2 at KAF.6, immediately downstream the dam, were similar with those measured in the epilimnion of the Itezhi Tezhi Reservoir (Fig. 3b). Unlike Kariba and Cahora Bassa, the Itezhi Tezhi Dam was not designed for power production, water being released from the epilimnion over the spillways, with rare bottom water withdrawals only during low storage (Zurbrügg et al., 2012). For the Kafue Gorge Reservoir, since no measurements were carried out in-, or immediately below the dam, we can only speculate the existence of a large CO_2 pool, both in the epilimnion and hypolimnion of the reservoir (given the inflow concentrations of over 9000 ppm - at KAF.9) and the release to the river downstream of large amounts of GHGs. We can further speculate that much lower pCO_2 levels measured systematically at KAF.10 (65 km downstream of the dam) compared to upstream stations (Fig. 3b) are the effect of rapid outgassing of hypolimnetic pCO_2 through the narrow and steep Kafue Gorge (600 m drop over less than 30 km).

All abovementioned effects of wetlands, reservoirs and the distinct hydrology on the dynamics of CO_2 concentrations along the Kafue River can also explain the longitudinal patterns of CH_4 and N_2O, and in combination with the hydrological conditions which determine the degree of water exchange with floodplains, are responsible for part of their temporal variability (Fig. 4b, 4c).

pCO_2 of all our sampled rivers and streams were generally well above atmospheric concentrations and comparable with pCO_2 values observed in other African rivers (i.e. Tendo, Aby, Oubangui, Tana, Athi-Galana-Sabaki rivers, see Koné et al., 2009; Bouillon et al., 2009, 2014; Tamooh et al., 2013; Marwick et al., 2014). However, values were well below global levels of tropical rivers and streams given by Aufdenkampe et al. (2011) (median 3600 and

4300 ppm, respectively), except for the Shire River (mean and median 13350 ppm, n=2) (Fig. 3d). This may be explained by the fact that global CO_2 levels for tropical aquatic systems originates mostly from studies on the Amazon River basin where "blackwater" rivers prevails. With pCO_2 in the surface water of the Itezhi Tezhi Reservoir above atmospheric concentration (mean 1174, median 1127 ppm), and substantially higher than both Kariba (mean 267, median 275 ppm) and Cahora Bassa reservoirs (mean 219, median 192 ppm), its level was still lower than literature-based median value for tropical lakes and reservoirs of 1900 ppm suggested by Aufdenkampe et al. (2011) (Fig. 3d). Undersaturated CO_2 conditions in surface waters such as of the Kariba and the Cahora Bassa reservoirs have being previously described for other reservoirs in Africa (Bouillon et al., 2009; Tamooh et al., 2013). Overall CH_4 concentrations in the Zambezi River mainstem (mean 769 nmol L^{-1}), higher than those of its major tributaries and reservoirs (Fig. 4d) were on average much higher than those measured in other African river systems such as the Oubangui River (~160 nmol L^{-1}, Bouillon et al., 2014), the Tana River (~160 nmol L^{-1}, Bouillon et al., 2009), the Galana River and several steams in Kenya (250 and 180 nmol L^{-1}, respectively, Marwick et al., 2014), and three rivers in Ivory Coast (Comoé: 206 nmol L^{-1}, Bia: 238 nmol L^{-1}, and Tanoé: 345 nmol L^{-1}, Koné et al., 2010). A comparable range was also observed in tributaries of the Oubangui (~740 nmol L^{-1}, Bouillon et al., 2014) and in the Athi-Galana-Sabaki River system in Kenya (~790 nmol L^{-1}, Marwick et al., 2014). With the exception of the Shire River where low N_2O concentrations of ~2.7 nmol L^{-1} could be explained by denitrification, mean N_2O range in the Zambezi River Basin (6.2 – 7.5 nmol L^{-1}, Fig. 5d) was similar to those of the Oubangui River mainstem and its tributaries (7.5 and 9.9 nmol L^{-1}, respectively, Bouillon et al., 2009). However, locally elevated concentrations linked to high anthropogenic N inputs have been recorded in the Athi-Galana-Sabaki River system in Kenya (up to 26 nmol L^{-1}, Marwick et al., 2014).

3.5 Dissolved inorganic carbon and its stable isotope signature

DIC in freshwater can be differentiated into two fractions with distinct origins and behaviors: carbonate alkalinity, mostly in the form of bicarbonate ions (HCO_3^-) which comes from soil and bedrock weathering, and dissolved CO_2, which results from respiration in soils, groundwaters, river sediments and waters column (Meybeck, 1987; Amiotte-Suchet et al., 1999). As the relative proportion of the two DIC fractions (and concentrations) depends greatly on the lithology of the drainage basin, rivers draining carbonate-rich watersheds would typically have high DIC concentrations (well above 1 mmol L^{-1}) of which HCO_3^- represents the major fraction compared to dissolved CO_2 (Meybeck, 1987). In these hard waters, characterized by high pH and high conductivity, HCO_3^- contributes to the majority of the TA. In contrast, rivers draining non-carbonate rocks and/or soils with high organic content would have lower DIC concentrations (well below 1 mmol L^{-1}), of which dissolved CO_2 commonly represents the dominant fraction (Abril et al., 2015). Characterized by low pH and low conductivity, these acidic, organic rich waters (soft or black waters) generally contain high DOC levels, sometimes exceeding DIC concentrations (Rantakari and Kortelainen, 2008; Whitfield et al., 2009; Einola et al., 2011), and organic acid anions contribute importantly to the TA (Driscoll et al., 1989; Hemond, 1990; Hunt et al., 2011; Abril et al., 2015).

The DIC values in all our sampled rivers (mean 1.32 mmol L^{-1}) together with conductivity (mean 140 µS cm^{-1}) and pH values (mean 7.61) may suggest the carbonate-rich lithology of the basin. However, low DIC, pH and conductivity values in the headwaters and their increasing patterns downstream along both the Zambezi and the Kafue rivers during all campaigns (data in the supplementary material) suggest either different chemical weathering rates or/and that a proportion of HCO_3^- may also come from silicate rock weathering. This is also suggested by the overall good correlation of TA with the sum of Ca^{2+} and Mg^{2+} (r^2=0.84, Fig. 6a) and the rather weak relationship (r^2=0.18) with DSi (Fig. 6b). To distinguish between

642 the contribution of silicate and carbonate weathering to the HCO_3^-, we applied the simple
643 stoichiometric model of Garrels and Mackenzie (1971) which calculates the contribution of
644 carbonate weathering (TA_{carb}) to TA from Ca^{2+} and Mg^{2+}, and the contribution of silicate
645 weathering (TA_{sil}) to TA from DSi according to:
646
647 $$TA_{carb} = 2\times([Ca^{2+}]+[Mg^{2+}]-[SO_4^{2-}]) \quad (R1)$$
648
649 $$TA_{sil} = [DSi]/2 \quad (R2)$$
650
651 While SO_4^{2-} in reaction (1) allows to account for Ca^{2+} originating from dissolution of gypsum
652 ($CaSO_4$), its contribution was ignored due to the absence of SO_4^{2-} measurements. However,
653 occurrence of gypsum in the Zambezi Basin is sporadic and mostly as nodules in a clay-rich
654 dambo within the Kafue Flats (Briggs and Mitchell, 1991), and in the upper catchment of
655 Shire River (downstream of Lake Malawi; Ashton at al., 2001). We acknowledge that the
656 approach used is prone to several caveats, such as the occurrence of weathering of Mg-rich
657 silicates such as olivine or the presence of SO_4^{2-} derived from the oxidation of pyrite or
658 elemental sulfur in organic sediments. However, it is difficult to fully address these issues
659 given for instance the lack of information on the lithology of catchment, and a more in depth
660 investigation of rock weathering is beyond the scope of the present study.
661 Nevertheless, application of the Garrels and Mackenzie (1971) model shows a
662 significant positive relationship between the modeled TA (TA_{Carb}+TA_{Sil}) and observed TA
663 (r^2=0.87, n=103) for all measured tributaries, reservoirs and Zambezi mainstem samples with
664 most of the data points falling on the 1:1 line (Fig. 7a). Exception from this pattern is found
665 on the upper most two sites of the Kafue River (KAF.1 and KAF.2) during 2013 dry
666 campaign where modeled TA is twice as high as the observed TA (Fig. 7a) due to unusually

667 high Ca^{2+} (1860 and 1360 µM) and Mg^{2+} (1035 and 1250 µM). Such high values during low
668 flow period, also linked to low pH (around 6) and low conductivity (5.4 and 33 µS cm^{-1},
669 respectively), found in this area of intense mining activities (mostly copper and cobalt) could
670 be the result of effluent discharge from the processing plants or leaking of contaminated water
671 from the extraction pits, tailings and slag dumps. The contribution of carbonate rock
672 weathering estimated as the percentage of TA_{Carb} ($\%TA_{Carb}$) to the total modeled TA
673 (TA_{Carb}+TA_{Sil}) in all samples ranged between 28 and 97% (mean 88%) (Fig. 7b). The strong
674 (r^2=0.88), positive, exponential relationship between $\%TA_{Carb}$ and TA (Fig. 7b) and the
675 general increase in $\%TA_{Carb}$ along the Zambezi mainstem (data not shown) may indicate a
676 lower contribution of carbonate rock weathering in the more humid forest areas of the
677 northwestern basin compared to the mostly open grassland areas and savannah in the south
678 and towards the ocean.

679 $\delta^{13}C_{DIC}$ in aquatic systems varies over a large range, being primarily controlled by
680 both in-stream and watershed processes (Finlay and Kendall, 2007). Marine carbonates have a
681 $\delta^{13}C$ close to 0‰ whereas $\delta^{13}C$ of atmospheric CO_2 is about −7.5‰ (Mook et al., 1983). The
682 $\delta^{13}C$ of soil CO_2 depends on the signature of the organic matter being mineralized, and are
683 expected lie within the range bracketed by d13C signatures for C3 vegetation (~-28 ‰) and
684 C4 vegetation (~-12 ‰). While in-stream CO_2 uptake during aquatic primary production and
685 degassing of CO_2 along the river course, make $\delta^{13}C_{DIC}$ less negative, the addition of respired
686 CO_2 (with isotopic signature similar with the organic C substrate) and the increasing
687 contribution of HCO_3^- (compared to CO_2) lowers the $\delta^{13}C_{DIC}$ (Finlay and Kendall, 2007).
688 While carbon in HCO_3^- which originates from silicate rock weathering comes exclusively
689 from CO_2 and will thus have a ^{13}C-depleted signature, carbonate weathering leads to more
690 ^{13}C-enriched $\delta^{13}C_{DIC}$, since half of the C in HCO_3^- is then derived from $CaCO_3$ and the half
691 from CO_2.

692 The overall $\delta^{13}C_{DIC}$ values in all our samples ranged from −21.9‰ at the Zambezi
693 source (during 2013 dry season campaign) to -1.8‰ in the Kariba and the Cahorra Bassa
694 reservoirs (during 2013 wet season), suggesting the occurrence of various C sources as well as
695 in-stream processes. The overall average value of −7.3‰ and the good relationship between
696 $\delta^{13}C_{DIC}$ and DSi:Ca^{2+} molar ratio, which explains 88% of the variability in $\delta^{13}C_{DIC}$, point
697 towards the influence of the relative importance of carbonate versus silicate mineral
698 weathering (Fig. 7c). However, the increase in $\delta^{13}C_{DIC}$ along the Zambezi mainstem (Fig. 7d)
699 alongside with an increase in POC in the lower Zambezi (data not shown), mostly laterally
700 derived but also partially in-river produced (as suggested by increased primary production
701 rates) points out to the interplay between downstream degassing and the degradation of the
702 organic matter in controlling $\delta^{13}C_{DIC}$ along the Zambezi River. A clear and instant effect of
703 degassing with a fast increase in $\delta^{13}C$ of the remaining DIC pool explained by the ^{13}C-
704 depletion of the CO_2 fraction relative to HCO_3^- and CO_3^{2-} (Doctor et al., 2008), can be best
705 seen at the Victoria Falls where during 2012 wet campaign we noticed a rapid increase in
706 $\delta^{13}C_{DIC}$ from −8.5 to −6.9 ‰ (Fig. 7d) coinciding with a decrease in pCO_2 from 2500 to 640
707 ppm (Fig. 3a). Similar CO_2 degassing effects on $\delta^{13}C_{DIC}$ were observed also downstream of
708 the Barotse floodplains (ZBZ.5 to ZBZ.6, 195 km) and downstream of the Chobe swamps
709 (ZBZ.7 to ZBZ.8, 74 km) where, during the same 2012 wet campaign, the drop in pCO_2 from
710 7560 to 1890 ppm and 6307 to 2500 ppm, respectively, was accompanied by an increase in
711 $\delta^{13}C_{DIC}$ from −8.5 to −6.9‰ and from −7.0 to −6.2‰, respectively (Fig. 3a, Fig. 7d). Ranging
712 between −4.1 and −1.8‰ (mean −2.9‰), the $\delta^{13}C_{DIC}$ values in the surface waters of the
713 Kariba and the Cahora Bassa reservoirs were highest among all samples during all three
714 campaigns (Fig. 7d). Associated with mostly undersaturated CO_2 conditions and negative CO_2
715 fluxes (Fig. 3a, Fig. 9a), R rates (in the order of ~0.8 µmol C L^{-1} h^{-1}) not different than
716 riverine values, and P rates (~25.0 µmol C L^{-1} h^{-1}) half the river values, the higher $\delta^{13}C_{DIC}$

values found in both reservoirs on the Zambezi can be primarily explained by the atmospheric CO_2 uptake during primary production, a process capable of generating strong diel variations (Parker et al., 2005). Slightly lower $\delta^{13}C_{DIC}$ values (−7.1 to −3.0‰, mean −5.2‰) characterized the surface water of the Itezhi Tezhi reservoir on the Kafue river. The observed $\delta^{13}C_{DIC}$ enrichment in the Itezhi Tezhi reservoir with increasing distance from the river inflow correlated with a gradual decrease in pCO_2, and comparable R rates (~0.7 µmol C L^{-1} h^{-1}) but higher P (~48.4 µmol L^{-1} h^{-1}) suggest the combined effect of P and CO_2 evasion (mostly originating with river inflow). While $\delta^{13}C_{DIC}$ in the Kafue River (−7.3±1.7‰, n=26, excluding the Itezhi Tezhi reservoir) was not significantly different from that of the Zambezi mainstem (−7.7±3.6‰, n=42, excluding the Kariba and the Cahora Bassa reservoirs), $\delta^{13}C_{DIC}$ values of smaller tributaries were significantly lower. The $\delta^{13}C_{DIC}$ values of the Kabompo (−10.7±0.7‰, n=3), Lunga (−9.8±1.0‰, n=5), Luangwa (−9.4±1.0‰, n=8), Lunsemfwa (−8.9±1.7‰, n=4) and Mazoe tributaries (−9.4‰, n=1) would suggest that in addition to carbonate weathering, there is a substantial increased contribution of soil CO_2 from C4 vegetation. Intermediate $\delta^{13}C_{DIC}$ values between reservoirs and tributaries were measured in the Shire River (−5.1±2.4‰, n=2) which drains the soft-water Lake Malawi. These isotopically enriched $\delta^{13}C_{DIC}$ values there coupled with highest recorded pCO_2 concentrations (mean 13350 ppm, Fig. 3d) must be explained by exceptionally high CO_2 degassing rates of over 23000 mg C m^{-2} d^{-1}, up to one order of magnitude larger than all other measured fluxes (Fig. 9a).

3.6 Diurnal variation in GHG concentrations

To account for the importance of diel fluctuations on the investigated biogeochemical parameters, we performed a 24-h sampling campaign at station ZBZ.11 on the Zambezi River between 22 and 23 November 2013 (dry season). Measurements show a small gradual

increase in water temperature (of 0.7 °C) from midday to midnight follow by a decrease (of 0.6 °C) between midnight and 9 a.m. when temperature started rising again (Fig. 8a, b). Similar sinusoidal patterns were observed over the same time period for DO (increased saturation with 7%, decreased with 5% followed by increase), pH (increased from 6.95 to 7.32, decrease to 7.21 followed by increase), and $\delta^{13}C_{DIC}$ (increased from −6.4 to −5.5‰, decrease to −6.1‰ followed by increase) (Fig. 8c, d, e). In contrast, a reverse pattern was recorded for pCO_2 which gradually decreased 30% (from 1655 to 1180 ppm) from midday to midnight (~40 ppm h^{-1}) and increased 30% (up to 1430 ppm) until 9 a.m. (~30 ppm h^{-1}), when values start slowly decreasing with the onset of primary production (Fig. 8g). Following pCO_2 pattern, DIC decreased 0.1 mmol L^{-1} (12%) between 12 a.m. and 12 p.m., and increased 0.03 mmol L^{-1} (3%) between 12 p.m. and 9 a.m. (Fig. 8f). While CH_4 followed the general pattern of pCO_2 (decreasing with 270 µmol L^{-1} and increasing with 150 µmol L^{-1} or ~25 µmol L^{-1} h^{-1}), N_2O showed no distinct diurnal variations (Fig. 8h, i). While these patterns provide clear evidences of diel variations of physico-chemical parameters, likely caused by variations in the relative magnitude of P and R, their overall influence on the river biogeochemistry appears to be rather small. As, for obvious logistical reasons, we have sampled exclusively during day time, the observed diel fluctuations suggest that, if anything, we may have possibly overestimated various parameters (i.e. dissolved gas concentrations and fluxes) by maximum 10 to 15%. To our knowledge, most existent studies which involved *in situ* measurements and data collection have been performed in the same manner, and are therefore subject to the same limitations.

3.7 CO_2 and CH_4 fluxes

Driven by supersaturation in CO_2 and CH_4 with respect to atmospheric equilibrium (Fig. 3, Fig. 4), the Zambezi River and all sampled tributaries were net sources of CO_2 and CH_4 to the

767 atmosphere. However, levels are well below the global emission range proposed by
768 Aufdenkampe et al. (2011) and Bastviken et al. (2011) for tropical rivers and streams (Fig. 9a,
769 b). Overall mean CO_2 and CH_4 fluxes of the Zambezi River of 3380 mg C m^{-2} d^{-1} (median
770 1409) and 48.5 mg C m^{-2} d^{-1} (median 12.4) were not different from those of the Kafue River
771 of 3711 mg C m^{-2} d^{-1} (median 1808) and 67.8 mg C m^{-2} d^{-1} (median 14.7) (Fig. 9). CO_2 fluxes
772 along the Zambezi mainstem were generally lower during 2013 dry season (mean 623 mg C
773 m^{-2} d^{-1}) compared to fluxes of the 2012 and 2013 wet season campaigns (mean 3280 and 5138
774 mg C m^{-2} d^{-1}, respectively). The opposite situation was observed for CH_4 where measured
775 fluxes during 2013 wet campaign (no CH_4 fluxes were measured during 2012 wet season)
776 (mean 26.5 mg C m^{-2} d^{-1}) were significantly lower compared to the 2013 dry season (mean
777 92.7 mg C m^{-2} d^{-1}). Singular events of negative CO_2 fluxes on the Zambezi mainstem were
778 measured only during 2013 dry season campaign at ZBZ.6 and ZBZ. 13 (mean -23 and -33
779 mg C m^{-2} d^{-1}, respectively), and corresponded to riverine pCO_2 values of 300 and 421 ppm,
780 respectively (Fig. 3a). Similar situation of undersaturated riverine CO_2 level was encountered
781 also on the Kafue River only during 2013 dry season (at KAF.4, 330 ppm, Fig. 3b) but no
782 reliable flux rate was determined there due to unusual, irregular fluctuations of CO_2
783 concentrations inside the floating chamber. With the exception of this, all other measured CO_2
784 fluxes on the Kafue River were positive, and fluxes of the dry season 2013 (mean 3338 mg C
785 m^{-2} d^{-1}) were not significantly different from those of the two wet seasons (mean 2458 and
786 5355 C m^{-2} d^{-1}, respectively). As in the case of the Zambezi River, CH_4 fluxes along the
787 Kafue were also higher during 2013 dry season (mean 149.5 mg C m^{-2} d^{-1}) compared to the
788 2013 wet season (mean 16.8 mg C m^{-2} d^{-1}). Chamber measurements provide the combined
789 CH_4 flux resulting from both ebullitive and diffusive fluxes. Since CH_4 concentrations during
790 the dry season were not higher compared to the wet season (Fig. 4a, b), the most likely
791 explanation for the higher CH_4 rates during low water level observed along both Zambezi and

Kafue rivers relates to higher contribution of ebullitive fluxes. This is consistent with higher CH_4 ebullitive fluxes during low waters than during high and falling waters in the Amazonian rivers (Sawakuchi et al., 2014). Higher contribution of CH_4 ebullition during 2013 dry campaign is further supported by the comparison between total CH_4 flux (measured with the floating chamber) and the estimated diffusive CH_4 flux (F) from the interfacial mass transfer mechanism from water to air expressed as:

$$F = k \times (C_w - C_{eq}) \quad (2)$$

where k is the gas transfer velocity back calculated from the measured CO_2 flux and normalized to a Schmidt number (Sc) of 600 ($k_{600} = k \times (600/Sc)^{-1/2}$), and C_w and C_{eq} are dissolved gas concentrations in the surface water and in the air, scaled by solubility to the value it would have when in the equilibrium with the atmosphere. Assuming that the difference between the computed (diffusive) and measured CH_4 flux is purely due to ebullition, the comparison suggests that on average, 73% of measured CH_4 fluxes during the 2013 wet campaign along both the Zambezi and the Kafue river were due to diffusive processes and only 27% originated from ebullition. In contrast, ebullition during the 2013 dry campaign accounted for up to 77% of measured CH_4 fluxes. This is in agreement with the contribution of CH_4 ebullition of more than 50% of total CH_4 emissions among different Amazonian rivers and seasons (Sawakuchi et al., 2014).

The k_{600} computed from CO_2 chamber flux measurements (on drift) ranged from 0.2 to 6.3 cm h^{-1} (mean 2.7, median 2.3 cm h^{-1}) for the Zambezi River, from 0.4 to 7.9 cm h^{-1} (mean 2.1, median 1.7 cm h^{-1}) for the Kafue River, and between 0.6 and 6.2 cm h^{-1} (mean 3.1, median 3.4 cm h^{-1}) for all other tributaries. These values are close to the k of ~3 cm h^{-1} suggested by Cole and Caraco (2001) for large rivers but well below the median global values

817 proposed by Aufdenkampe et al. (2011) for tropical rivers and streams (12.3 and 17.2 cm h^{-1},
818 respectively), and the basin-wide average value of 20.6 cm h^{-1} for the Zambezi given by
819 Raymond et al. (2013). The higher value given by Raymond et al. (2013) corresponds to the
820 average of the whole river network including low order streams that typically have high *k*
821 values (Raymond et al., 2012) while our data was obtained mainly in high order tributaries
822 and mainstem. Few extreme *k* values (20.3 to 79.7 cm h^{-1}) obtained from the flux chamber
823 measurements performed on static mode (non drift) and explained by additional induced
824 turbulence by the water rushing against the chamber walls have been excluded from the
825 overall calculations. In situ experiments, mostly on the Congo River, designed to explore the
826 effect of additionally induced turbulence by the chamber walls on the flux chamber
827 determination in rivers, and performed both on static mode at various water velocities as well
828 as drift mode, suggest a clear, linear dependency of *k* on the velocity of water relative to the
829 floating chamber (Cristian R. Teodoru, unpublished data).

830 It is worth noting that the highest CO_2 fluxes along both Zambezi and Kafue rivers
831 were found mostly in or downstream of wetlands and floodplains (i.e. ~12500 mg C m^{-2} d^{-1},
832 downstream of the Barotse floodplains; >4000 mg C m^{-2} d^{-1} downstream of the Chobe
833 swamps; >12700 mg C m^{-2} d^{-1} in and downstream of the Kafue Flats) and in the delta
834 (>10000 mg C m^{-2} d^{-1}). Such high outgassing rates there are consistent with findings of
835 studies on the Amazonian river-floodplains system which stress the importance of wetlands
836 and floodplains on river biogeochemistry, especially on the CO_2 fluxes (Richey et al., 2002;
837 Abril et al., 2014). Moreover, the highest CO_2 and CH_4 fluxes of the Zambezi mainstem
838 (>20000 mg C m^{-2} d^{-1} and 154 mg C m^{-2} d^{-1}, respectively) were consistently measured at
839 ZBZ.18 immediately downstream the confluence with the Shire River. The only outlet of
840 Lake Malawi, the Shire River passes through a large stagnant waters complex of
841 swamp/mashes (the Elephant Marsh) before it joins the Zambezi River. With mean CO_2 and

842 CH_4 fluxes in the region of 23100 mg C m^{-2} d^{-1} and 1170 mg C m^{-2} d^{-1}, respectively, and
843 much higher than the global emission level for tropical streams (Fig. 9), the Shire River
844 represented a hotspot for both CO_2 and CH_4 emissions. Average CO_2 and CH_4 emissions for
845 all tributaries (excluding the Kafue River) of 4790 mg C m^{-2} d^{-1} (median 2641) and 180.7 mg
846 C m^{-2} d^{-1} (median 10.1), respectively, while higher than of the Zambezi mainstem, are still
847 well below the global level for tropical rivers and streams (Fig. 9). In contrast, the two
848 reservoirs on the Zambezi Rivers (the Kariba and the Cahora Bassa), were both sinks of
849 atmospheric CO_2 (mean −141 and −356 mg C m^{-2} d^{-1}), but small sources of CH_4 (5.2 and 1.4
850 mg C m^{-2} d^{-1}, respectively) (Fig. 9). A different situation was encountered for the much
851 smaller Itezhi Tezhi Reservoir on the Kafue River, where average CO_2 emission in the range
852 of 737 mg C m^{-2} d^{-1} (median 644), approaches the global emission rate for tropical lakes and
853 reservoirs (Fig. 9a), but the CH_4 flux of 25.8 mg C m^{-2} d^{-1} is still below the reported global
854 range (Fig. 9b).

855 Using the GWP factor of CH_4 of 34 CO_2-equivalent (CO_2eq) for 100 years time
856 horizon (IPCC, 2013), mean CH_4 fluxes of the Zambezi and Kafue rivers mainstem would
857 translate into 1650 and 2305 mg C-CO_2eq m^{-2} d^{-1}, respectively, slightly lower but comparable
858 with the magnitude of CO_2 fluxes (3380 and 3711 mg C m^{-2} d^{-1}, respectively). However, CH_4
859 emissions from tributaries (without Kafue) and reservoirs of 6145 and 460 mg C-CO_2eq m^{-2} d^{-1}
860 , respectively, are distinctly higher, surpassing the equivalent CO_2 emissions by 1.5 and 2
861 fold, respectively.

862 The Victoria Falls on the upper Zambezi form another important hotspot for GHG
863 emissions. A simple calculation suggests that the instant and almost complete degassing of
864 CO_2 (75%) and CH_4 (97%) during 2013 wet season campaign as the water dropped over 108
865 m depth of the fall at a rate of 1245 m^3 s^{-1}, released approximately 75 t C d^{-1} as CO_2 and 0.4 t
866 C d^{-1} as CH_4. For CO_2, this is equivalent with what the Zambezi River would emit over an

867 area of more than 20 km^2 or over a stretch of 33 km length for an average river width of 600
868 m.
869
870 **3.8 C mass balance**
871 We constructed a simple C mass balance over the study period for the Zambezi River which
872 consists of three main components: (i) the outgassed load to the atmosphere, (ii) the C load to
873 the sediment, and (iii) the C export load to the ocean (Fig. 10). The GHG load to the
874 atmosphere was calculated as the product between surface area and the measured areal CO_2
875 and CH_4 fluxes. Surface area of rivers was estimated by mapping each river sector between
876 two sampling points using the geometrical applications in Google Earth Pro. Each sector was
877 then multiplied with the corresponding average flux of the two bordering sampling points and
878 results were summed up to calculate the overall GHG load (in kt C yr^{-1}). Estimates of river
879 surface area were restricted to the Zambezi mainstem (1879 km^2 without reservoirs) and the
880 Kafue river (287 km^2 without reservoirs) (Table 1a) for which we have a relatively good
881 longitudinal distribution of data, and where an extrapolation between sampling stations can be
882 made with some confidence. Back calculated from the overall riverine CO_2 and CH_4 loads to
883 the atmosphere divided by total river surface, area weighted-average fluxes for the Zambezi
884 River (4291 mg C m^{-2} d^{-1} and 45.0 mg C m^{-2} d^{-1}, respectively) and the Kafue River (2962 mg
885 C m^{-2} d^{-1} and 20.0 mg C m^{-2} d^{-1}, respectively) (Table 1a) are higher for the Zambezi and lower
886 for the Kafue than corresponding arithmetic average fluxes. In the absence of reliable areal
887 estimates for the rest of hydrological network, fluxes of all other sampled tributaries, even
888 potentially important, were not included in the overall emission calculation. GHG emissions
889 for reservoirs were calculated as a product between the corresponding mean fluxes and
890 surface area (Table 1a). The surface area of the Kariba (5364 km^2), Cahora Bassa (2670 km2),
891 Itezhi Tezhi (364 km^2) and Kafue Gorge (13 km^2) reservoirs were taken from the literature

892 (Beilfuss and dos Santos, 2001; Kunz et al., 2011a, b; Kling et al., 2014). CO_2 and CH_4
893 emissions for the Kafue Gorge Reservoir were extrapolated using mean fluxes of the Itezhi
894 Tezhi Reservoir.

895 C deposition was estimated considering only removal in reservoirs while deposition in
896 rivers, in the absence of direct measurements, was assumed negligible. C deposition in the
897 Kariba and the Itezhi Tezhi reservoirs of 120 and 16 kt C yr^{-1}, respectively, were taken from
898 available literature data (Kunz et al., 2011a, b) while C retention in the Cahora Bassa and the
899 Kafue Gorge reservoirs of 60 and 0.6 kt C yr^{-1}, respectively, were extrapolated from the rates
900 of the Kariba and the Itezhi Tezhi reservoirs (Table 1a).

901 The export load to the ocean (Table 1b) was computed as the product between the
902 annual flow rate (Q) and the average POC (2.6 mg L^{-1}), DOC (2.2 mg L^{-1}) (own unpublished
903 data) and DIC (30.8 mg L^{-1}) measured at the two stations in the delta, close to the river mouth
904 (ZBZ.19 and ZBZ.20). Lacking direct discharge measurements at the river mouth over the
905 study period, an annual average flow rate of 3779 m^{-3} s^{-1} was calculated from the existing
906 literature data of 3424 and 4134 m^3 s^{-1} (Beilfuss and dos Santos, 2001; World Bank, 2010).

907 Mass balance calculations suggest a total C yield of 7215 kt yr^{-1} (or 5.2 t C km^{-2} yr^{-1})
908 of which: (i) 38% (2779 kt C yr^{-1}) is annually emitted into the atmosphere, mostly in the form
909 of CO_2 (98%), (ii) 3% (196 kt C yr^{-1}) is removed by sedimentation in the main reservoirs, and
910 (iii) 59% (4240 kt C yr^{-1}) is exported to the ocean, mostly in the form of DIC (87%), with
911 organic C component accounting only for a small fraction (7% POC and 6% DOC) (Fig. 10).
912 Even potential large uncertainties for the overall balance may occur from the lack of direct
913 discharge measurements at the river mouth, the limitation of riverine GHG emission only to
914 the mainstem of the Zambezi and the Kafue river, and from missing data on C removal by
915 sedimentation in rivers, the overall picture is rather consistent with previous figures of global
916 C budgets (Cole et al., 2007; Battin et al., 2009). It is worth mentioning that our relatively

lower C emissions component of the balance compared to global budgets, is the direct result of atmospheric CO_2 uptake by the surface waters of the Kariba and Cahora Bassa reservoirs (Table 1). Despite their relatively low uptake rates (-141 and -356 mg C m^{-2} d^{-1}, respectively, Table 1), the huge areal extent of the two reservoirs, which accounts for more than 76% of the total estimated aquatic surface used in the budget, lowered the overall outgassed load by 20%. This in turn, reduces the relative contribution of the C emission component of the balance by 6%. In other words, if both reservoirs on the Zambezi were C neutral (most likely situation since the atmospheric CO_2 uptake must be compensated by rapid release of hypolimnetic CO_2 pool with the disruption of thermal stratification during the winter period in July-August), the relative contribution of emissions, deposition and export to the total budget would reach 43%, 3%, and 54%, respectively. The influence of reservoirs on riverine C budget can be clearly seen in the case of Kafue River where a similar balance approach would suggest a reverse situation with emissions surpassing the downstream export by almost two-fold. With both Itezhi Tezhi and Kafue Gorge reservoirs contributing 1/3 to the total emissions of 417 kt C yr^{-1} (Table 1a), a C burial rate of 17 kt C yr^{-1} (Table 1a) and an export load of around 258 kt C yr^{-1}, this would translate into a similar C yield of 4.4 t C km^{-2} yr^{-1} (691 kt yr^{-1}) but the balance between emission, deposition and export components would be shifted to 60%, 3%, and 37%, respectively.

Failing to incorporate C emissions from the entire hydrological network of the Zambezi River basin clearly underestimates the overall C outgassing load. For instance, using a total rivers and streams area of 7325 km^2 for the Zambezi basin (excluding lakes and reservoirs) derived from a limnicity index of 0.42% and a total catchment area of 1730000 km^2 (Raymond et al., 2013), and a mean CO_2 and CH_4 flux of 3630 and 32.5 mg C m^{-2} d^{-1}, respectively (average between Zambezi and Kafue values, Table 1a), GHG emission from the entire Zambezi River network would reach ~9780 kt C yr^{-1}. Taking further into account C

emissions and sinks in reservoirs, and the export load to the ocean, a simple calculation would suggest a total C yield of ~13710 kt yr^{-1} (~10 t C km^{-2} yr^{-1}) of which GHG emissions account for up to 68% while the export load represent less than 30%. Moreover, the relative contribution of GHG to the present C budget would increase considerably if taking into account emissions from the highly productive systems such as wetlands and floodplains of which influence on the biogeochemistry of the river has been clearly demonstrated throughout this work and elsewhere (Aufdenkampe et al., 2011; Abril et al., 2014). For instance, a rough estimate of C emissions from the only four major floodplain/wetlands in the basin (the Barotse floodplain: 7700 km^2, the Chobe swamps: 1500 km^2, the Lukanga swamps: 2100 km^2, and the Kafue Flats: 6500 km^2) calculated using our fluxes measured on the river downstream of their locations, and applied to merely half of their reported surface area and over only the seasonal flooding period (half-year) would add to the overall emissions an extra 16000 kt C yr^{-1}. Assuming no further C deposition in these areas, the incorporation of wetlands into the present budget would increase the total C yield to 17 t C km^{-2} yr^{-1} (or 23400 kt C yr^{-1}) while the relative contribution of degassing would reach 81% (19000 kt C yr^{-1}) . While the flux term of our budget may represent a low limit estimate, further research and more quantitative data are needed in order to improve our understanding of the links between river and wetlands and to better constrain the role of aquatic systems as a whole in both regional and global C budgets.

4 Concluding remarks

Overall, results of this catchment-scale study demonstrate that riverine GHGs, despite their interannual and seasonal variations, appeared to be mainly controlled by the connectivity with floodplains/wetlands, the presence of rapids/waterfalls and the existence of large man-made structures along the aquatic continuum. While TA, $\delta^{13}C_{DIC}$ and DSi:Ca^{2+} values suggest the

967 importance of both carbonate weathering as well as in-stream processes in controlling riverine
968 DIC, the co-variation of pCO_2 with CH_4 suggest that both dissolved gases in this river system
969 are largely controlled by organic matter degradation processes. While comparable with other
970 studied river systems in Africa, the range in GHG concentrations and fluxes in the Zambezi
971 River Basin were generally below the reported global median for tropical rivers, streams and
972 lakes/reservoirs, for which the current empirical dataset is strongly biased towards studies of
973 the Amazon River Basin. While GHG concentrations and evasion rates may generally be
974 higher in the Amazon Basin, upscaling from that region to the whole tropical zone is prone to
975 high uncertainties. Our C mass balance for the Zambezi River suggest that GHG emission to
976 the atmosphere represents less than 40% of the total budget, with C export to the ocean
977 (mostly as DIC) being the dominant component (59%). However, the importance of GHG
978 emissions in the overall budget is likely underestimated since our analyses do not take into
979 account fluxes from the entire hydrological network (i.e. all tributaries), and since potentially
980 large emissions that occur in the seasonally flooded wetlands and floodplains have not been
981 estimated.
982
983 ***Acknowledgements***. Funding for this work was provided by the European Research Council
984 (ERC-StG240002, AFRIVAL - African river basins: catchment-scale carbon fluxes and
985 transformations, http://ees.kuleuven.be/project/afrival/) and the Research Foundation Flanders
986 (FWO-Vlaanderen, travel grants K2.011.12N and K2.266.13N to Cristian R. Teodoru).
987 Alberto V. Borges is a senior research associate at the FRS-FNRS. We thank Zita Kelemen
988 (KU Leuven) for technical and laboratory assistance, Marc-Vincent Commarieu (University
989 of Liège) for the TA measurements, Kristin Coorevits ans Stijn Baeken (KU Leuven) for ICP-
990 MS measurements, Peter Salaets (KU Leuven) for nutrient analyses, and Stephan Hoornaert
991 and Sandro Petrovic (University of Liège) who carried out part of the CH_4 measurements. We

992 thank all generous and helpful people (Maurice Diamond, Sam Talbot, Tony Weber, Ann-
993 Marie Butzelaar, Andrew Peter Dekker, and many others) for logistical support during
994 sampling. Three anonymous reviewers provided useful comments and suggestions that
995 allowed to improve the previous version of the manuscript.

References

Abril, G., Martinez. J. M., Artigas, L. F., Moreira-Turcq. P., Benedetti, M. F., 5 Vidal, L., Meziane, T., Kin, J. H., Bernardes, M. C., Savoye, N., Deborde, J., Souza, E. L., Albéric, P., Landim de Souza, M. F., and Roland, F.: Amazon River carbon dioxide outgassing fuelled by wetlands, Nature, 505, 395-398, doi:10.1038/nature12797, 2014.

Abril, G., Bouillon, S., Darchambeau, F., Teodoru, C. R., Marwick, T. R., Tamooh, F., Omengo, F. O., Geeraert, N., Deirmendjian, L., Polsenaere, P., and Borges, A. V.: Technical Note: Large overestimation of pCO_2 calculated from pH and alkalinity in acidic, organic-rich freshwaters, Biogeosciences, 12(1), 67-78, doi:10.5194/bg-12-67-2015, 2015.

Amiotte-Suchet, P., Aubert, D., Probst, J. L., Gauthier-Lafaye, F., Probst, A., Andreux, F., and Viville, D.: $\delta^{13}C$ pattern of dissolved inorganic carbon in a small granitic catchment: the Strengbach case study (Vosges mountains, France), Chem. Geol., 159, 129-145, 1999.

Ashton, P. J., Love, D., Mahachi, H., and Dirks, P. H. G. M.: An overview of the impact of mining and mineral processing operations on water resources and water quality in the Zambezi, Limpopo and Olifants Catchments in Southern Africa. Contract Report to the Mining, Minerals and Sustainable Development (SOUTHERN AFRICA). Project by CSIR-Environmentek, Pretoria, South Africaand Geology Department, University of Zimbabwe, Harare, Zimbabwe, Rep. ENV-P-C 2001–042, 336 pp., available at: http://pubs.iied.org/pdfs/G00599.pdf (last access: 15 September 2014), 2001.

Aufdenkampe, E. K., Mayorga, E., Raymond, P. A., Melack, J. M., Doney, S. C., Alin, S. R., Aalto, R. E., and Yoo, K.: Rivers key to coupling biogeochemical cycles between land, oceans and atmosphere, Front. Ecol. Environ. 9, 53-60, doi:10.1890/100014, 2011.

1019 Bastviken, D., Tranvik, L. J., Downing, J. A., Crill, P. M., and Enrich-Prast, A.: Freshwater
1020 methane emissions offset the continental carbon sink, Science, 331, 6013,
1021 doi:10.1126/science.1196808, 2011.

1022 Battin, T. J., Luyssaert, S., Kaplan, L. A., Aufdenkampe, A. K., Richter, A., and Tranvik, L.
1023 J.: The boundless carbon cycle, Nat. Geosci., 2, 598-600, doi:10.1038/ngeo618, 2009.

1024 Beilfuss, R. and dos Santos, D.: Patterns of hydrological change in the Zambezi Delta,
1025 Mozambique. Working Paper #2: Program for the sustainable management of Cahora
1026 Bassa Dam and the Lower Zambezi Valley, USA, International Crane Foundation,
1027 Direcção Naçional de Aguas, Mozambique, 2001.

1028 Berggren, M., Lapierre, J-F, del Giorgio, P. A.: Magnitude and regulation of bacterioplankton
1029 respiratory quotient across freshwater environmental gradients, The ISME Journal 6, 984-
1030 993, doi:10.1038/ismej.2011.157, 2012.

1031 Bouillon, S., Abril, G., Borges, A. V., Dehairs, F., Govers, G., Hughes, H. J., Merckx, R.,
1032 Meysman, F. J. R., Nyunja, J., Osburn, C., and Middelburg, J. J.: Distribution, origin and
1033 cycling of carbon in the Tana River (Kenya): a dry season basin-scale survey from
1034 headwaters to the delta, Biogeosciences, 6, 2475-2493, doi:10.5194/bg-6-2475-2009, 2009.

1035 Bouillon, S., Yambélé, A., Spencer, R. G. M., Gillikin, D. P., Hernes, P. J., Six, J., Merckx,
1036 R., and Borges, A. V.: Organic matter sources, fluxes and greenhouse gas exchange in the
1037 Oubangui River (Congo River basin), Biogeosciences, 9, 2045-2062, doi:10.5194/bg-9-
1038 2045-2012, 2012.

1039 Bouillon, S., Yambélé, A., Gillikin, D. P., Teodoru, C. R., Darchambeau, F., Lambert, T., and
1040 Borges, A. V.: Contrasting biogeochemical characteristics of the Oubangui River and
1041 tributaries (Congo River basin), Sci. Rep.,4, 5402, doi:10.1038/srep05402, 2014.

1042 Briggs, D. A. and Mitchell, C. J.: Mineralogy and beneficiation of some industrial minerals
1043 from Zambia, Zamb, J. Appl. Earth Sci., 5, 18-27, 1991.

1044 Butman, D. and Raymond, P. A.: Significant efflux of carbon dioxide from streams and rivers
1045 in the United States, Nat. Geosci., 4, 839-842, doi:10.1038/ngeo1294, 2011.

1046 Cole, J. J. and Caraco, N. F.: Carbon in catchments: connecting terrestrial carbon losses with
1047 aquatic metabolism, Mar. Freshwater Res., 52, 101-110, 2001.

1048 Cole, J. J., Prairie, Y. T., Caraco, N. F., McDowell, W. H., Tranvik, L. J., Striegl, R. G.,
1049 Duarte, C. M., Kortelainen, P., Downing, J. A., Middelburg, J. J., and Melack, J.: Plumbing
1050 the global carbon cycle: integrating inland waters into the terrestrial carbon budget,
1051 Ecosystems, 10, 171-184, 2007.

1052 Chenje, M.: State of the Environment Zambezi Basin 2000, SADC, IUCN, ZRA, and
1053 SARDC, Maseru, Lusaka and Harare, 334 pp., ISBN 978-1-77910-009-2, 2000.

1054 Dauchez, S., Legendre, L., and Fortier, L.: Assessment of simultaneous uptake of nitrogenous
1055 nutrients (^{15}N) and inorganic carbon (^{13}C) by natural phytoplankton populations, Mar.
1056 Biol., 123, 651-666, 1995.

1057 Doctor, D. H., Kendall, C., Sebestyen, S. D., Shanley, J. B., Ohte, N., and Boyer, E. W.:
1058 Carbon isotope fractionation of dissolved inorganic carbon (DIC) due to outgassing of
1059 carbon dioxide from a headwater stream, Hydrol. Process., 22, 2410-2423, 2008.

1060 Driscoll, C. T., Fuller, R. D., Schecher, W. D.: The role of organic acids in the acidification of
1061 surface waters in the eastern US, Water Air Soil Poll., 43, 21–40, 1989.

1062 Einola, E., Rantakari, M., Kankaala, P., Kortelainen, P., Ojala, A., Pajunen, H., Mäkelä, S.,
1063 and Arvola, L.: Carbon pools and fluxes in a chain of five boreal lakes: a dry and wet year
1064 comparison, J. Geophys. Res., 116, G03009, doi:10.1029/2010JG001636, 2011.

1065 Finlay, J. C.: Controls of streamwater dissolved inorganic carbon dynamics in a forested
1066 watershed, Biogeochemistry, 62, 231-252, doi:10.1023/A:1021183023963, 2003.

1067 Finlay, J. C. and Kendall, C.: Stable isotope tracing of temporal and spatial variability in
1068 organic matter sources to freshwater ecosystems, in: Stable Isotopes in Ecology and
1069 Environmental Science, 2nd edn., edited by: Michener, R. and Lajtha, K., Blackwell
1070 Publishing, Oxford, UK, 2007.

1071 Garrels, R. M. and Mackenzie, F. T.: Evolution of Sedimentary Rocks, W. W. Norton, New
1072 York, 397 pp., 1971.

1073 Gillikin, D. P. and Bouillon, S.: Determination of $\delta^{18}O$ of water and $\delta^{13}C$ of dissolved
1074 inorganic carbon using a simple modification of an elemental analyzer – isotope ratio mass
1075 spectrometer (EA-IRMS): an evaluation, Rapid Commun. Mass Sp., 21, 1475-1478, 2007.

1076 Guasch, H., Armengol, J., Martí, E., and Sabater, S.: Diurnal variation in dissolved oxygen
1077 and carbon dioxide in two low-order streams, Water Res., 32, 1067–1074,
1078 doi:10.1016/S0043-1354(97)00330-8, 1998.

1079 Guérin, F., Abril, G., Richard, S., Burban, B., Reynouard, C., Seyler, P., and Delmas, R.:
1080 Methane and carbon dioxide emissions from tropical reservoirs: significance of
1081 downstream rivers. Geophys. Res. Lett., 33, L21407, doi: 10.1, 029/2006GL027929, 2006.

1082 Hemold, H. F.: Acid neutralizing capacity, alkalinity, and acid-base status of natural waters
1083 containing organic acids, Environ. Sci. Technol., 24, 1486-1489, 1990.

1084 Hunt, C. W., Salisbury, J. E., and Vandemark, D.: Contribution of non-carbonate anions to
1085 total alkalinity and overestimation of pCO_2 in New England and New Brunswick rivers,
1086 Biogeosciences, 8, 3069-3076, doi:10.5194/bg-8-3069-2011, 2011.

1087 IPCC: Working group I contribution to the fifth assessment report (AR5) of the
1088 intergovernmental panel on climate change, in: Climate Change 2013: The Physical

1089 Science Basis, Cambridge University Press, Cambridge, United Kingdom and New York,
1090 NY, USA, 1552 pp., 2013.

1091 Kling, G. W, Kipphut, G. W., and Miller, M. C.: Arctic lakes and streams as gas conduits to
1092 the atmosphere: implications for tundra carbon budgets, Science, 251, 298-301,
1093 doi:10.1126/science.251.4991.298, 1991.

1094 Kling, H., Stanzel, P., and Preishuber, M.: Impact modelling of water resources development
1095 and climate scenarios on Zambezi River discharge, J. Hydrol. Reg. Stud., 1, 17-43 2014.

1096 Koné, Y. J. M., Abril, G., Kouadio, K. N., Delille, B., and Borges, A. V.: Seasonal variability
1097 of carbon dioxide in the rivers and lagoons of Ivory Coast (West Africa), Estuar. Coast.,
1098 32, 246-260, 2009.

1099 Koné, Y. J. M., Abril, G., Delille, B., and Borges, A. V.: Seasonal variability of methane in
1100 the rivers and lagoons of Ivory Coast (West Africa), Biogeochemistry, 100, 21-37, 2010.

1101 Kunz, M. J., Anselmetti, F. S., Wuestm, A., Wehrli, B., Vollenweider, A., Thuring, S., and
1102 Senn, D. B.: Sediment accumulation and carbon, nitrogen, and phosphorus deposition in
1103 the large tropical reservoir Lake Kariba (Zambia/Zimbabwe), J. Geophys. Res., 116,
1104 G03003, doi:10.1029/2010JG001538, 2011a.

1105 Kunz, M. J., Wuest, A., Wehrli, B., Landert, J., and Senn, D. B.: Impact of a large tropical
1106 reservoir on riverine transport of sediment, carbon and nutrients to downstream wetlands,
1107 Water Resour. Res., 47, W12531, doi:10.1029/2011WR010996, 2011b.

1108 Kunz, M. J., Senn, D. B., Wehrli, B., Mwelwa, E. M., and Wüest, A.: Optimizing turbine
1109 withdrawal from a tropical reservoir for improved water quality in downstream wetlands.
1110 Water Resour. Res, 49, 1-15. doi:10.1002/wrcr.20358), 2013.

1111 Lambert, T., Darchambeau, F., Bouillon, S., Alhou, B., Mbega, J - D, Teodoru, C. R., Nyoni,
1112 F. C., and A V Borges, A. V.: The effect of vegetation cover on the spatial and temporal

variability of dissolved organic carbon and chromophoric dissolved organic matter in large African rivers, submitted, 2015.

Lewis, E. and Wallace, D. W. R.: Program developed for CO_2 system calculations. ORNL/CDIAC-105, published by Carbon Dioxide Information Analysis Center, Oak Ridge National Laboratory, U.S. Department of Energy, Oak Ridge, Tennessee, 1998.

Ludwig, W., Probst, J.-L., and Kempe, S.: Predicting the oceanic input of organic carbon by continental erosion, Global Biogeochem. Cy., 10, 23-41, 1996.

Mann, P. J., Spencer, E. G. M., Dinga., B. J., Poulsen, J. R., Hernes, P. J., Fiske, G., Salter, M. E., Wang, Z. A., Hoering, K. A., Six, J., and Holmes, R. M.: The biogeochemistry of carbon across a gradient of streams and rivers within the Congo Basin, J. Geophys. Res.-Biogeo., 119, 687-702, 2014.

Marwick, T. R., Tamooh, F., Ogwoka, B., Teodoru, C., Borges, A. V., Darchambeau, F., and Bouillon, S.: Dynamic seasonal nitrogen cycling in response to anthropogenic N loading in a tropical catchment, Athi–Galana–Sabaki River, Kenya, Biogeosciences, 11, 443-460, doi:10.5194/bg-11-443-2014, 2014.

McCartney, M. P. and Houghton-Carr, H. A.: Modelling approach to assess inter-sectoral competition for water resources in the Kafue Flats, Zambia, Water Environ. J., 12, 101-106, doi:10.1111/j.1747-6593.1998.tb00157.x, 1998.

McCartney, M., Cai, X., and Smakhtin, V.: Evaluating the flow regulating functions of natural ecosystems in the Zambezi River Basin, IWMI Res. Rep. 148, International Water Management Institute (IWMI), Colombo, Sri Lanka, 59 pp., doi:10.5337/2013.206, 2013.

Mengis, M. R., Gächter, R., and Wehrli, B.: Sources and sinks of nitrous oxide (N_2O) in deep lakes, Biogeochemistry, 38, 281-301, 1997.

1136 Meybeck, M.: Global chemical-weathering of surficial rocks estimated from river dissolved
1137 loads, Am. J. Sci., 287, 401-428, 1987.

1138 Millero, F. J.: The thermodynamics of the carbonic acid system in seawater, Geochim.
1139 Cosmochim. Ac., 43, 1651-1661, 1979.

1140 Moore, A. E., Cotterill, F. P. D., Main, M. P. L., and Williams, H. B.: The Zambezi River, in:
1141 Large Rivers: Geomorphology and Management, edited by: Gupta, A., John Wiley & Sons,
1142 Ltd, Chichester, UK, 311-333, 2007.

1143 Mook, W. G., Koopmans, M., Carter, A. F., and Keeling, C. D.: Seasonal, latitudinal, and
1144 secular variations in the abundance and isotopic ratios of atmospheric carbon dioxide: 1.
1145 Results from land stations. J. Geophys. Res., 88, 10915-10933, 1983.

1146 Mook, W. G. and Tan, F. C.: Stable carbon isotopes in rivers and estuaries, in:
1147 Biogeochemistry of Major World Rivers, edited by: Degens, E. T., Kempe, S., and Richey,
1148 J. E. John Wiley, Hoboken, N. J., 245-264, 1991.

1149 Mumba, M. and Thompson, J. R.: Hydrological and ecological impacts of dams on the Kafue
1150 Flats floodplain system, southern Zambia, Phys. Chem. Earth, 30, 442-447, 2005.

1151 Parker, S. R., Poulson, S. R., Gammons, C. H., and Degrandpre, M. D.: Biogeochemical
1152 controls on diel cycling of stable isotopes of dissolved O_2 and dissolved inorganic carbon
1153 in the Big Hole River, Montana, Environ. Sci. Technol., 39, 7134-7140, 2005.

1154 Rantakari, M. and Kortelainen, P.: Controls of total organic and inorganic carbon in randomly
1155 selected Boreal lakes in varied catchments, Biogeochemistry, 91, 151-162, 2008.

1156 Raymond, P. A., Hartmann, J., Lauerwald, R., Sobek, S., McDonald, C., Hoover, M.,
1157 Butman, D., Striegl, R., Mayorga, E., Humborg, C., Kortelainen, P., Dürr, H., Meybeck,
1158 M., Ciais, P., and Guth, P.: Global carbon dioxide emissions from inland waters, Nature,
1159 503, 355–359, doi:10.1038/nature12760, 2013.

1160 Raymond, P. A., C. J. Zappa C. J., Butman, D., Bott, T. L., Potter, C., Mulholland, P.,
1161 Laursen, A. E., McDowell, W. H., and Newbold, D.: Scaling the gas transfer velocity and
1162 hydraulic geometry in streams and small rivers, Limnol. Oceanogr. Fluids Environ. 2: 41-
1163 53 DOI 10.1215/21573689-1597669, 2012.

1164 Richardson, D. C., Newbold, J. D., Aufdenkampe, A. K., Taylor, P. G., and Kaplan, L. A.:
1165 Measuring heterotrophic respiration rates of suspended particulate organic carbon from
1166 stream ecosystems, Limnol. Oceanogr.-Meth., 11, 247-261, 2013.

1167 Richey, J. E., Devol, A. H., Wofy, S. C., Victoria, R., and Riberio, M. N. G.: Biogenic gases
1168 and the oxidation and reduction of carbon in Amazon River and floodplain waters, Limnol.
1169 Oceanogr., 33, 551-561, 1988.

1170 Richey, J. E., Melack, J. M., Aufdenkampe, A. K., Ballester, V. M., and Hess, L.: Outgassing
1171 from Amazonian rivers and wetlands as a large tropical source of atmospheric CO_2,
1172 Nature, 416, 617-620, 2002.

1173 Richardson, D. C., Newbold, J. D., Aufdenkampe, A. K., Taylor, P. G. and L. A. Kaplan, L.
1174 A.: Measuring heterotrophic respiration rates of suspended particulate organic carbon from
1175 stream ecosystems. Limnol. Oceanogr. Meth., 11:247-261, doi: 10.4319/lom, 2013.

1176 SADC, SARDC, GRID-Arendal, and ZAMCOM: Zambezi River Basin Atlas of the Changing
1177 Environment. Southern African Development Community (SADC), Southern African
1178 Research and Documentation Centre (SARDC), United Nations Environment Programme
1179 (UNEP)/GRID-Arendal, Zambezi Watercourse Commission (ZAMCOM), Gaborone,
1180 Harare and Arendal, 134 pp., 2012.

1181 Sawakuchi, H. O., Bastviken, D., Sawakuchi, A. O., Krusche, A. V., Ballester, M. V. R., and
1182 Richey, J. E.: Methane emissions from Amazonian Rivers and their contribution to the
1183 global methane budget, Glob. Change Biol., 20, 2829-2840, doi:10.1111/gcb.12646, 2014.

1184 Schlünz, B. and Schneider, R. R.: Transport of organic carbon to the oceans by rivers:
1185 reestimating flux and burial rates, Int. J. Earth Sci., 88, 599-606, 2000.

1186 Tamooh, F., Van den Meersche, K., Meysman, F., Marwick, T. R., Borges, A. V., Merckx, R.,
1187 Dehairs, F., Schmidt, S., Nyunja, J., and Bouillon, S.: Distribution and origin of suspended
1188 matter and organic carbon pools in the Tana River Basin, Kenya, Biogeosciences, 9, 2905-
1189 2920, doi:10.5194/bg-9-2905-2012, 2012.

1190 Tamooh, F., Borges, A. V., Meysman, F. J. R., Van Den Meersche, K., Dehairs, F., Merckx,
1191 R., and Bouillon, S.: Dynamics of dissolved inorganic carbon and aquatic metabolism in
1192 the Tana River basin, Kenya, Biogeosciences, 10, 6911-6928, doi:10.5194/bg-10-6911-
1193 2013, 2013.

1194 Teodoru, C. R., del Giorgio, P., Prairie, Y. T., and Camire, M.: pCO_2 dynamics in boreal
1195 streams of northern Quebec, Canada, Global Biogeochem. Cy., 23, GB2012,
1196 doi:10.1029/2008GB003404, 2009.

1197 Teodoru, C. R., del Giorgio, P., and Prairie, Y. T.: Spatial heterogeneity of surface CO_2 fluxes
1198 in a newly created Eastmain-1 reservoir in northern Quebec, Canada, Ecosystems, 14, 28-
1199 46, doi:10.1007/s10021-010-9393-7, 2010.

1200 Tranvik, L. J., Downing, J. A., Cotner, J. B., Loiselle, S. A., Striegl, R. G., Ballatore, T. J.,
1201 Dillon, P., Finlay, K., Knoll, L. B., Kortelainen, P. L., Kutser, T., Larsen, S., Laurion, I.,
1202 Leech, D. M., McCallister, L. S., McKnight, D. M., Melack, J. M., Porter, J. A., Prairie, Y.
1203 T., Renwick, W. H., Roland, F., Sherman, B. S., Schindler, D. W., Sobeck, S., Tremblay,
1204 A., Vanni, M. J., Verschoor, A. M., von Wachenfelds, E., and Weyhenmeyer, G. A.: Lakes
1205 and reservoirs as regulators of carbon cycling and climate, Limnol. Oceanogr., 54, 2298-
1206 2314, doi:10.4319/lo.2009.54.6_part_2.2298, 2009.

1207 Waldron, S., Scott, E. M., and Soulsby, C.: Stable isotope analysis reveals lower-order river
1208 dissolved inorganic carbon pools are highly dynamic, Environ. Sci. Technol., 41, 6156-
1209 6162, doi:10.1021/es0706089, 2007.

1210 Wang, Z. A., Bienvenu, D. J., Mann, P. J., Hoering, K. A., Poulsen, J. R., Spencer, R. G. M.,
1211 and Holmes, R. M.: Inorganic carbon speciation and fluxes in the Congo River, Geophys.
1212 Res. Lett., 40, 511-516, doi:10.1002/grl.50160, 2013.

1213 Weiss, F. R. and Price, B. A.: Nitrous oxide solubility in water and seawater, Mar. Chem., 8,
1214 347-359, 1980.

1215 Weiss, R. F.: Determinations of carbon dioxide and methane by dual catalyst flame ionization
1216 chromatography and nitrous oxide by electron capture chromatography, J. Chromatogr.
1217 Sci., 19, 611-616, 1981.

1218 Wellington, J. H.: Southern Africa – a Geographic Study, vol. 1, Physical Geography,
1219 Cambridge University Press, Cambridge, 528 pp., 1955.

1220 Whitfield, P. H., Aherne, J., and Watmough, S.: Predicting the partial pressure of carbon
1221 dioxide in boreal lakes, Can. Water Resour. J., 34, 415-426, 2009.

1222 World Bank.: The Zambezi River Basin. A multi-sector investment opportunities analysis,
1223 vol. 3: State of the basin, published by the International Bank for Reconstruction and
1224 Development/The World Bank, 1818 H Street NW, Washington DC 20433, USA, 2010.

1225 Worrall, F., Burt, T., and Adamson, J.: Fluxes of dissolved carbon dioxide and inorganic
1226 carbon from an upland peat catchment: implications for soil respiration, Biogeochemistry,
1227 73, 515-539, doi:10.1007/s10533-004-1717-2, 2005.

1228 Zurbrügg, R., Wamulume, J., Kamanga, R., Wehrli, B., and Senn, D. B.: River-floodplain
1229 exchange and its effects on the fluvial oxygen regime in a large tropical river system
1230 (Kafue Flats, Zambia), J. Geophys. Res., 117, G03008, doi:10.1029/2011JG001853, 2012.

Yamamoto, S., Alcauskas, J. B., and Crozier, T. E.: Solubility of methane in distilled water and seawater, J. Chem. Eng. Data, 21, 78-80, 1976.

Tables

Table 1: a) Carbon emission estimates based on measured CO_2 and CH_4 fluxes (this work) and carbon removal by deposition in reservoirs based on available published data (Kunz et al., 2011a, b); b) Carbon export loads to the ocean calculated using average literature river discharge at the Zambezi Delta and POC, DOC and DIC concentrations (this work) measured at the river mouth (ZBZ.19 and ZBZ.20) during 2012 and 2013 wet season campaigns; and c) Carbon mass balance components including yield, emission, deposition and export. Data marked with * represent areal fluxes recalculated for the entire surface including reservoirs. Carbon deposition in the Kafue Gorge and Cahora Bassa reservoirs (**) were estimated assuming same deposition rates of the Itezhi Tezhi and the Kariba reservoirs. All loads are expressed in kt C yr^{-1} (1 kt = 10^3 metric tons).

a)

River/Reservoir	Area	CO_2 flux	CH_4 flux	CO_2	CH_4	Emission	Deposition
	[km^2]	[mg C m^{-2} d^{-1}]		[kt C yr^{-1}]			
Kafue River without reservoirs	287	2962	20.0	310	2.1	312	-
Itezhi Tezhi Reservoir	364	737	25.8	98	3.4	101	16
Kafue Gorge Reservoir	13	737	25.8	3	0.1	4	1**
Kafue River with reservoirs	***664***	***1698****	***23.3****	***411***	***5.6***	***417***	***17***
Zambezi River without reservoirs	1879	4291	45.0	2943	30.8	2974	-
Kariba Reservoir	5364	-141	5.2	-276	10.1	-266	120
Cahora Bassa Reservoir	2670	-356	1.4	-347	1.4	-346	60**
Zambezi River with reservoirs	***9913***	***641****	***11.7****	***2319***	***42.3***	***2362***	***180***
Zambezi & Kafue Rivers with reservoirs	**10576**	**707***	**12.4***	**2731**	**48.0**	**2779**	**196**

b)

River	Q	POC	DOC	DIC	POC	DOC	DIC
	[m^3 s^{-1}]	[mg L^{-1}]			[kt C yr^{-1}]		
Zambezi River at Delta	3779	2.6	2.2	30.8	306	263	3672

c)

	Yield	Emission	Deposition	Export	Emission	Deposition	Export
	[kt C yr^{-1}]				[%]		
Carbon Balance at Zambezi Delta	7215	2779	196	4240	38	3	59

Figures

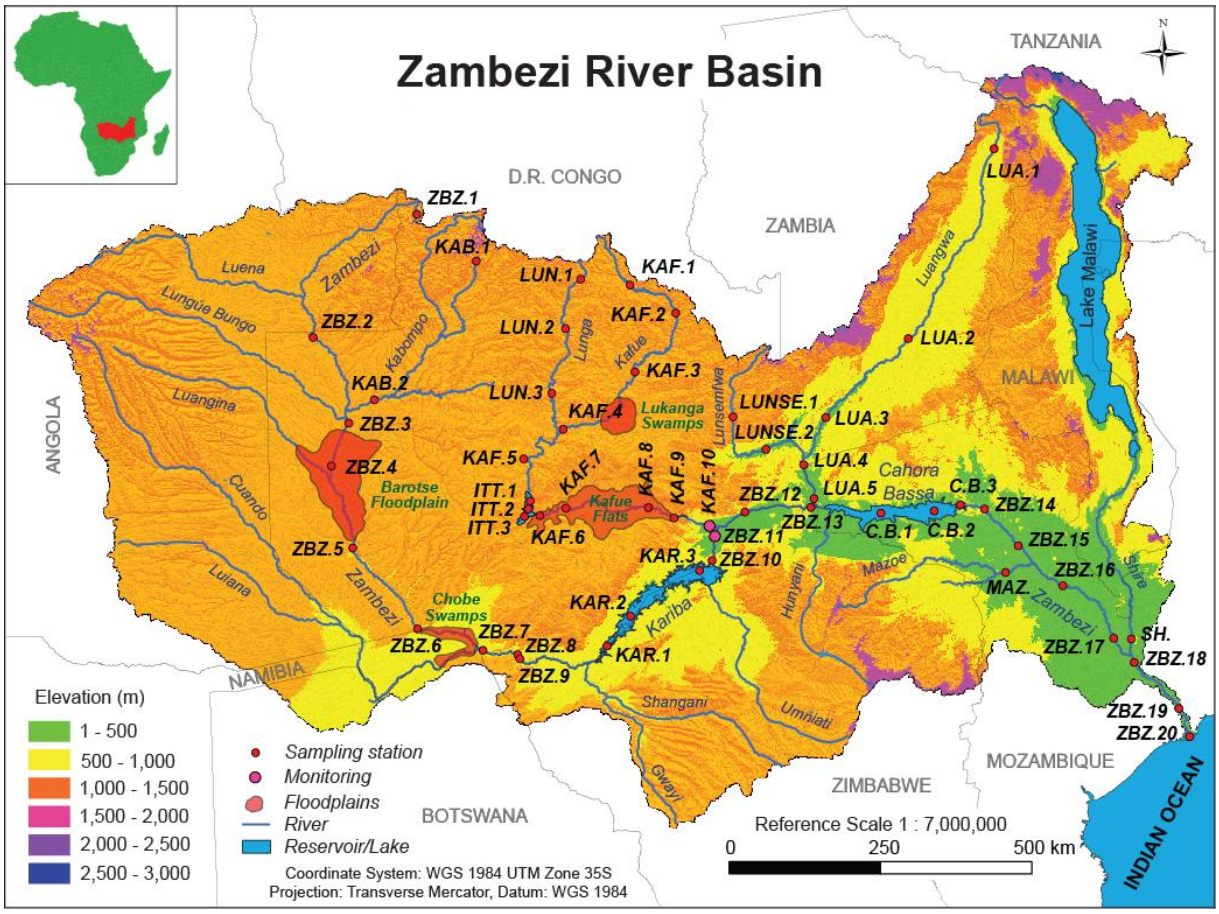

Fig. 1: Map of the Zambezi River Basin illustrating the location within Africa, the shared area of the basin within the eight African nations, the elevation gradient, the main hydrological network and the distribution of sampling sites along the Zambezi mainstem and major tributaries.

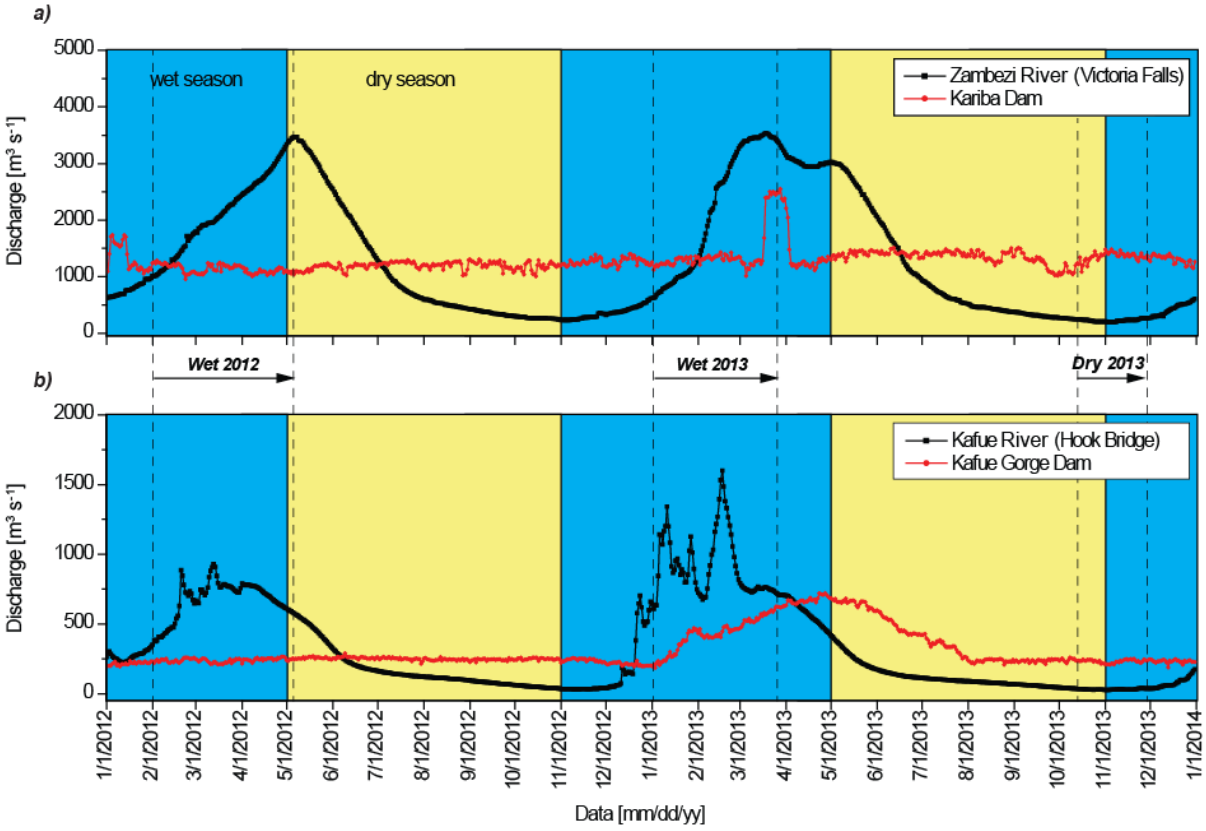

1248

1249 Fig. 2: Water discharge for: a) the Zambezi River at Victoria Falls power station and the
1250 disturbance of natural flow pattern by dam operation at Kariba Dam, and b) for the Kafue
1251 River at the Hook Bridge (upstream of the Itezhi Tezhi Reservoir) and the regulated flow at
1252 the Kafue Gorge Dam between January 2012 and January 2014 (data from Zambia Electricity
1253 Supply Corporation Limited, ZESCO).

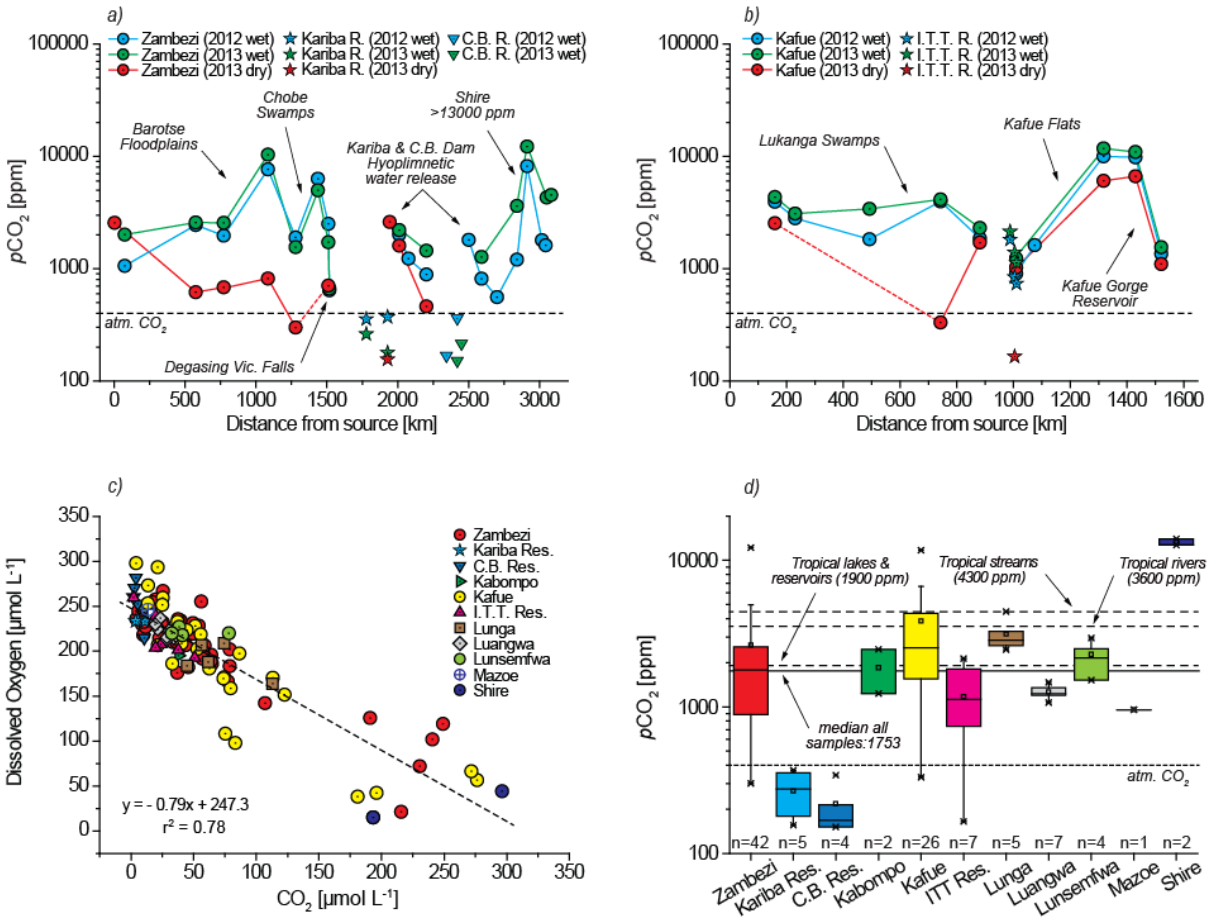

Fig. 3: Spatial and temporal variability of pCO_2 along: a) the Zambezi River including the Kariba Reservoir (Kariba R.) and Cahora Bassa Reservoir (C.B. R), and b) the Kafue River including the Itezhi Tezhi Reservoir (I.T.T. R.). Panel (c) shows the negative correlation between CO_2 and dissolved oxygen (µmol L^{-1}); and panel (d) shows the overall range in pCO_2 for the Zambezi River, tributaries and reservoirs. Box-plots show range, percentile, median, mean and outliers. The dotted line represents atmospheric CO_2 concentration while dashed lines represent global median pCO_2 values for tropical rivers, streams and lakes/reservoirs based on Aufdenkampe et al. (2011). Full line represents median pCO_2 value (1753 ppm) of all sites during the entire sampling period.

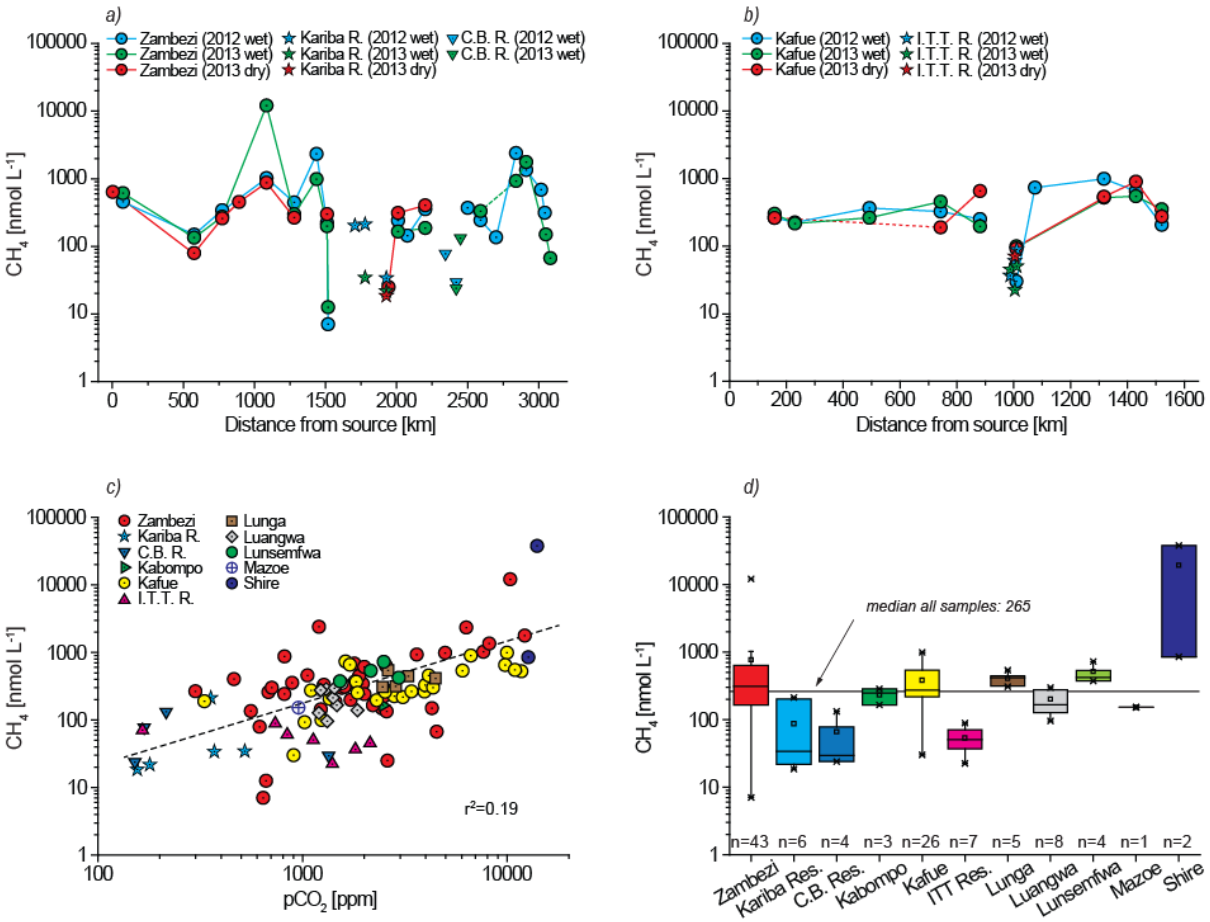

Fig. 4: Spatial and temporal variability of CH_4 along: a) the Zambezi mainstem including the Kariba Reservoir (Kariba R.) and Cahora Bassa Reservoir (C.B. R), and b) the Kafue River including the Itezhi Tezhi Reservoir (I.T.T. R.). Panel (c) shows the correlation between CH_4 and pCO_2; and panel (d) shows the overall (all campaigns) range CH_4 concentration for the Zambezi River, tributaries and reservoirs. Box-plot shows range, percentile, median, mean and outliers. Full line represents median CH_4 value (265 µmol L^{-1}) of all sites during the entire sampling period.

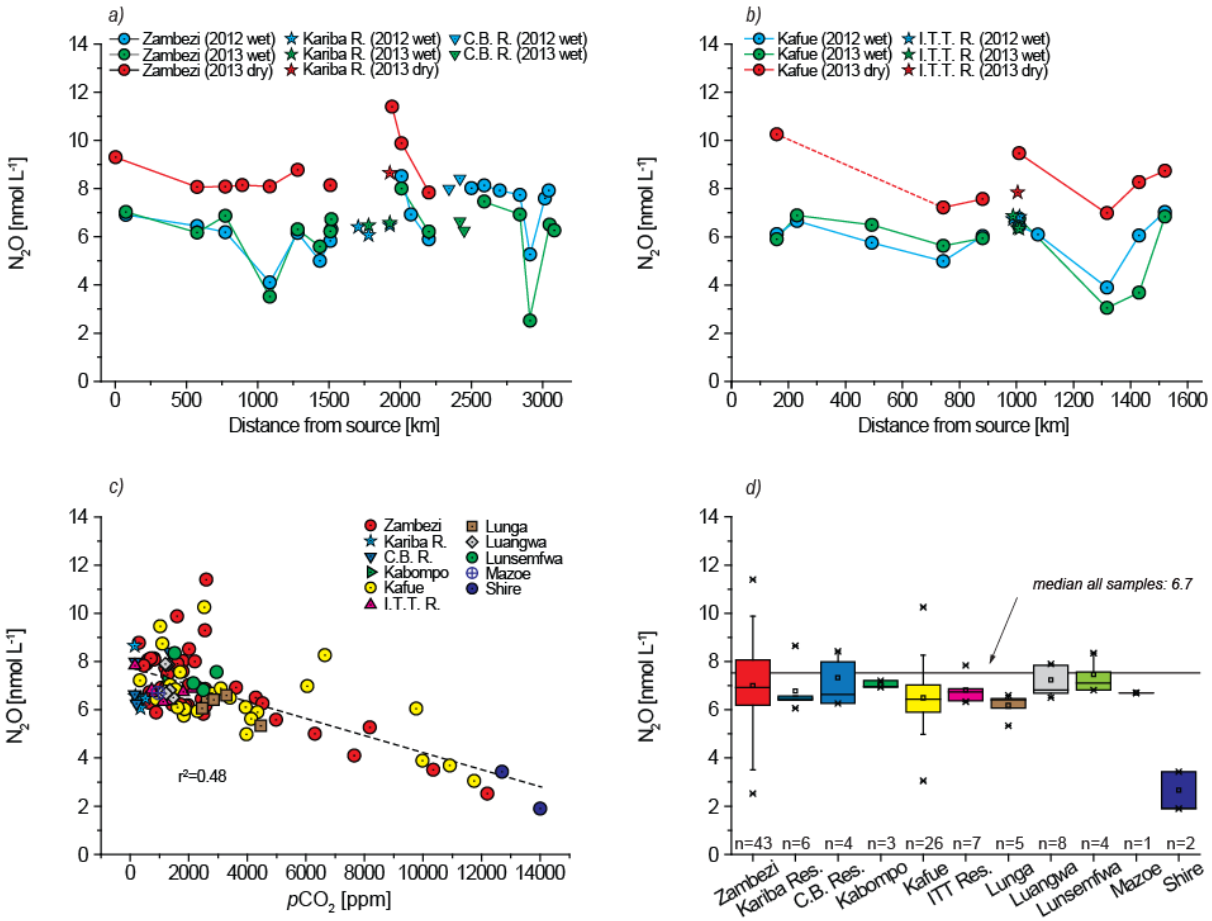

Fig. 5: Spatial and temporal variability of N_2O along: a) the Zambezi River including the Kariba Reservoir (Kariba R.) and Cahora Bassa Reservoir (C.B. R), and b) the Kafue River including the Itezhi Tezhi Reservoir (I.T.T. R.). Panel (c) shows the correlation between N_2O and pCO_2; and panel (d) shows overall (all campaigns) range N_2O concentration for the Zambezi River, tributaries and reservoirs. Box-plot shows range, percentile, median, mean and outliers. Full line represents median N_2O value (6.7 µmol L^{-1}) of all sites during the entire sampling period.

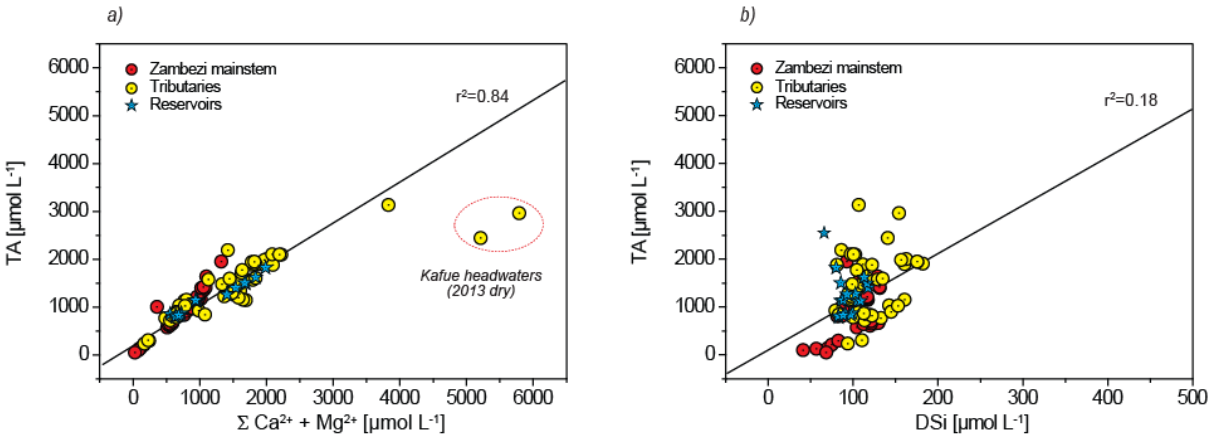

1280

1281 Fig. 6: Relationships between the observed total alkalinity (TA) and: a) the sum of Ca^{2+} and

1282 Mg^{2+}, and b) dissolved silica (DSi).

1283

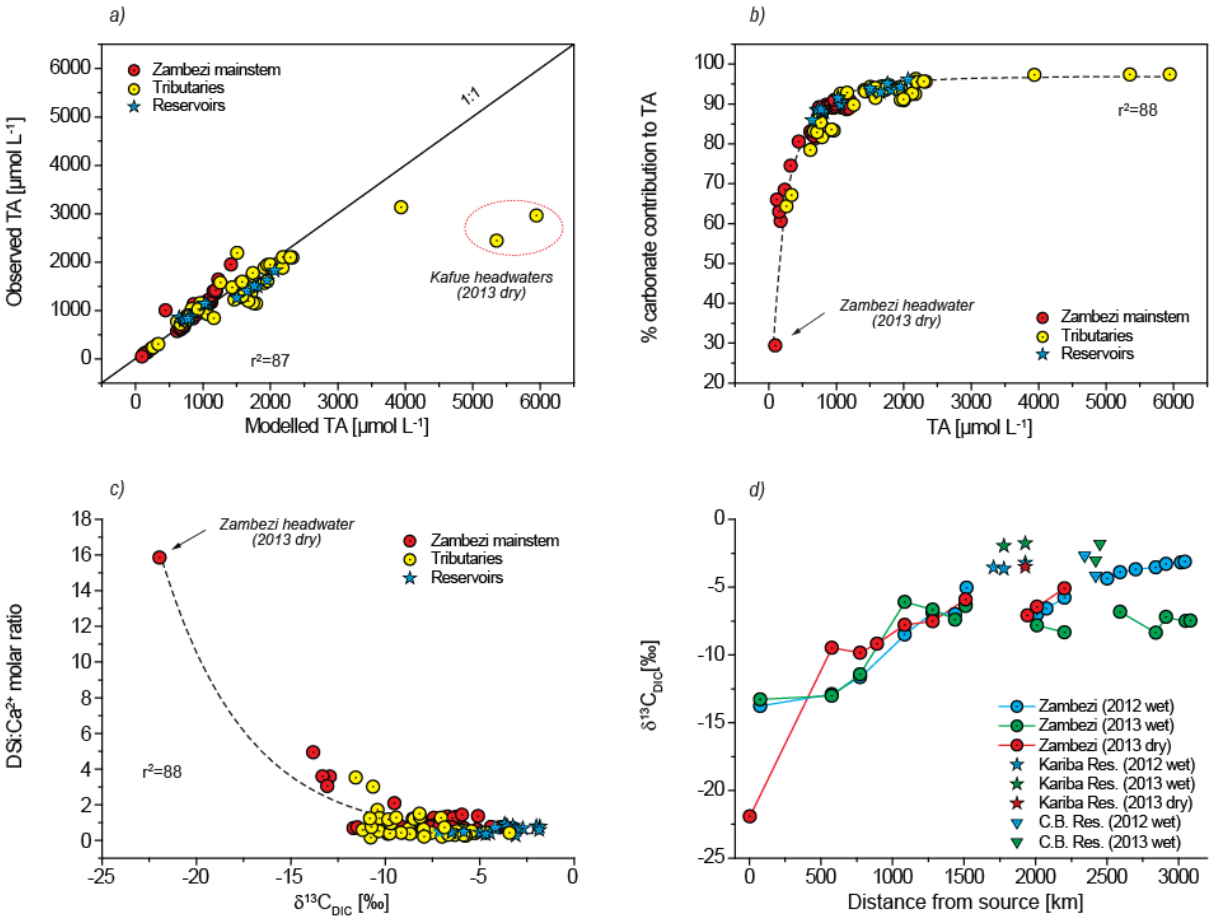

Fig. 7: Relationships between: a) modeled and observed total alkalinity (TA), b) the estimated contribution of TA derived from carbonate weathering to observed TA (see text for details), and c) isotopic signature of DIC ($\delta^{13}C_{DIC}$) to DSi:Ca^{2+} molar ratio. Panel (d) shows the spatio-temporal variability of $\delta^{13}C_{DIC}$ along the Zambezi mainstem.

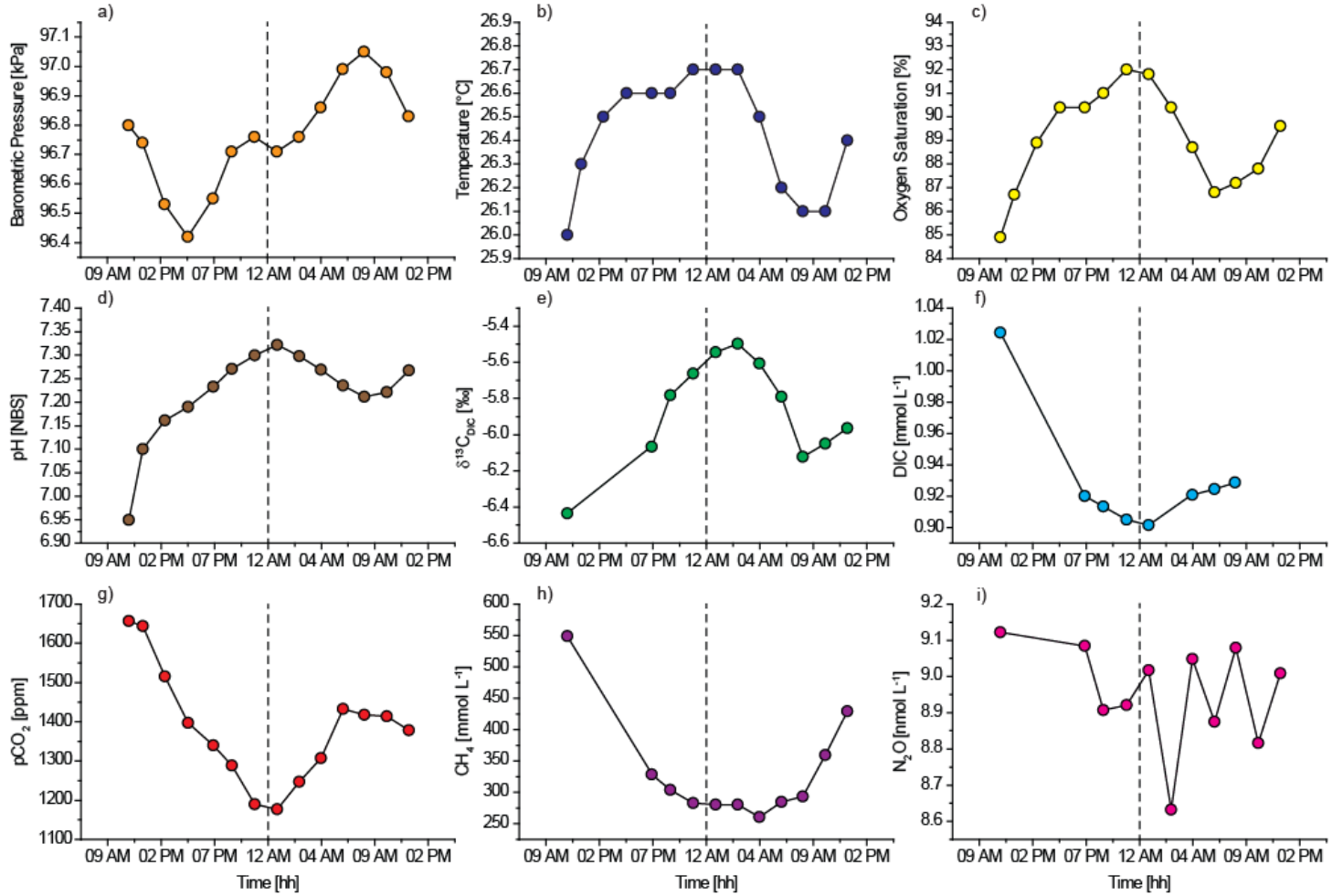

Fig. 8: Diel variations of: a) barometric pressure, b) temperature, c) dissolved oxygen saturation (%DO), d) pH, e) isotopic signature of dissolved inorganic carbon ($\delta^{13}C_{DIC}$), f) dissolved inorganic carbon concentrations (DIC), g) partial pressure carbon dioxide (pCO_2), h) methane (CH_4), and i) nitrous oxide (N_2O) measured at ZBZ.11 between 22 and 23 November 2013.

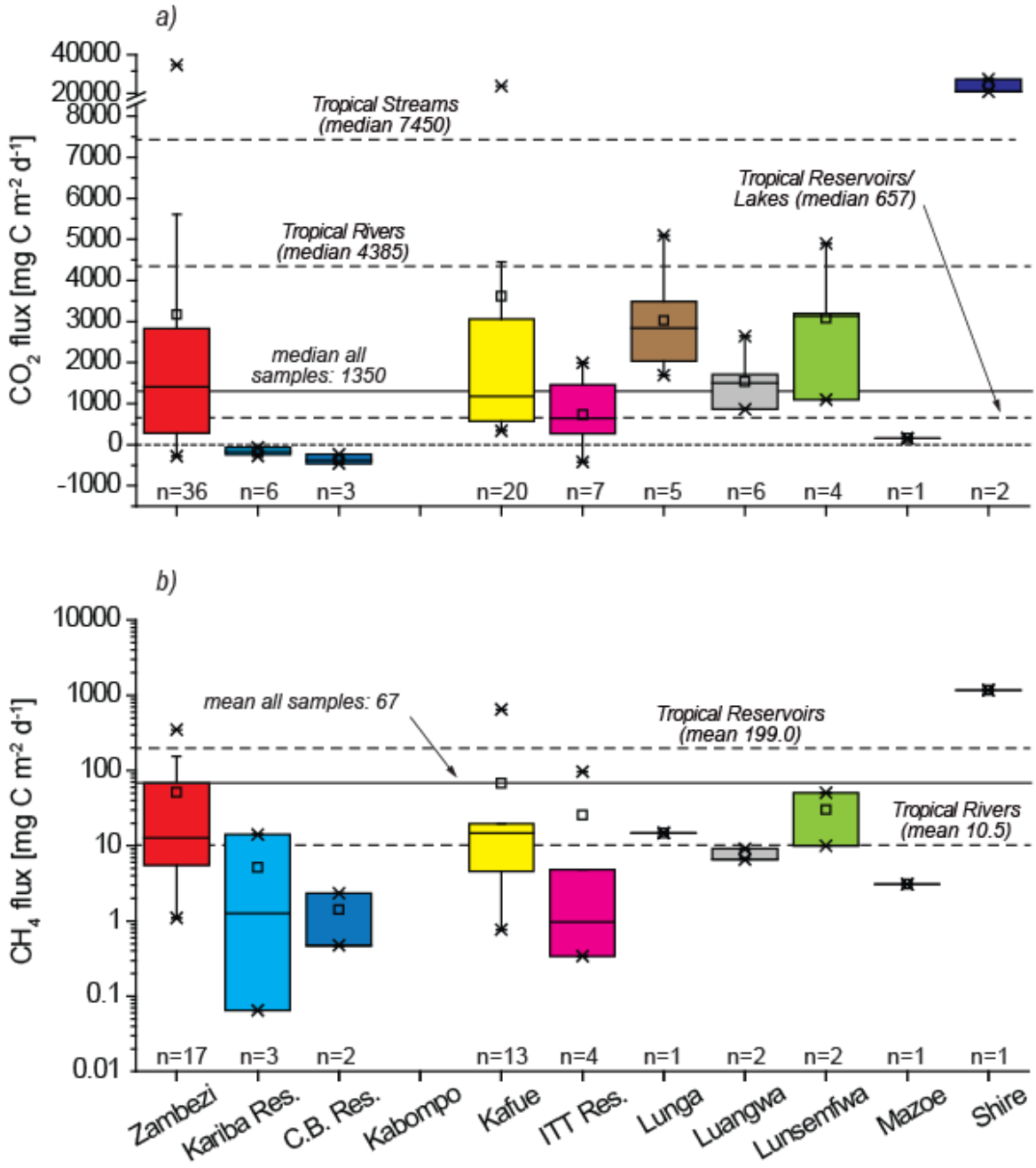

Fig. 9: Measured range in (a) CO_2 fluxes and (b) CH_4 fluxes (note the log scale in the latter) for the Zambezi mainstem, tributaries and reservoirs. Box-plots show the range, percentile, median, mean and outliers. Dashed lines in a) represent global median CO_2 efflux for tropical rivers, streams and lakes/reservoirs based on Aufdenkampe et al., 2011, while in b) it represents the global mean CH_4 emission for tropical rivers and reservoirs as suggested by Bastviken et al.(2011). Full lines represent median CO_2 emissions (a) and mean CH_4 flux (b) of all sites and over the entire sampling period.

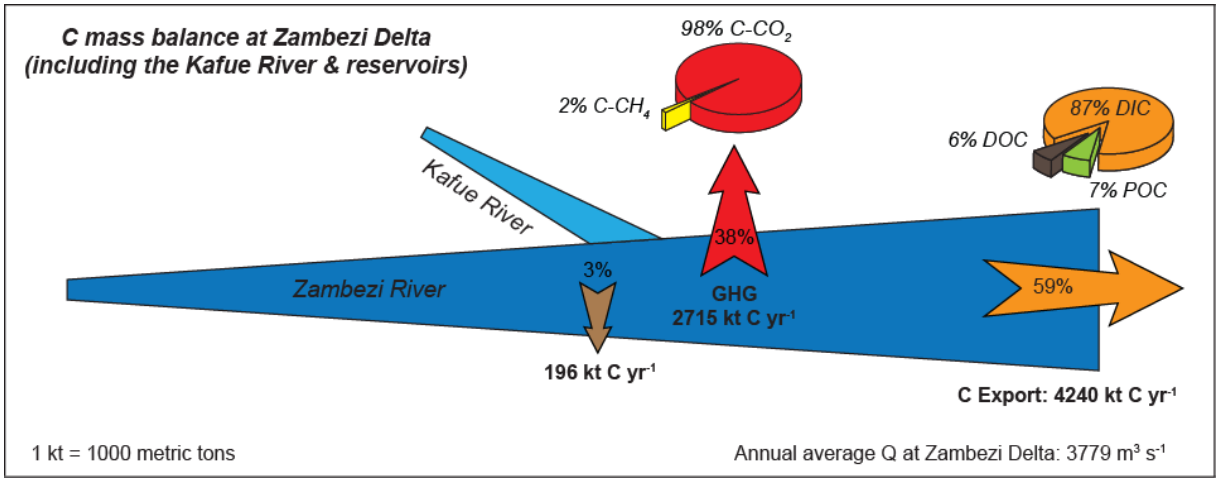

1301

1302 Fig. 10: Carbon mass budget for the Zambezi River. GHG emission component was
1303 calculated for a total surface area of 10,576 km^2 out of which Zambezi mainstem represents
1304 18%, Kafue River accounts for 3%, Itezhi Tezhi and Kafue Gorge reservoirs sum up to
1305 approximately 4%, while Kariba and Cahora Bassa reservoirs represent 75% (see Table 1).